

Astronomical calibration of the Paleocene time

Thomas Westerhold ^{a,*}, Ursula Röhl ^a, Isabella Raffi ^b, Eliana Fornaciari ^c,
Simonetta Monechi ^d, Viviana Reale ^d, Julie Bowles ^e, Helen F. Evans ^f

^a Center for Marine Environmental Sciences (Marum), University of Bremen, Leobener Strasse, 28359 Bremen, Germany

^b Facoltà di Scienze, Dipartimento di Geotecnologie per l'Ambiente e il Territorio, Università "G. d'Annunzio" di Chieti-Pescara, Campus Universitario, Via dei Vestini 31, Chieti Scalo, 66013, Italy

^c Dipartimento di Geologia, Paleontologia e Geofisica, Università di Padova, Via Giotto 1, 35137 Padova, Italy

^d Dipartimento di Scienze della Terra, Università di Firenze, Via La Pira 4, 50121 Firenze, Italy

^e Department of Geology and Geophysics, University of Hawaii, 1680 East-West Road, Honolulu, HI 96822, USA

^f Department of Geological Sciences, University of Florida, Gainesville, FL 32611, USA

Received 27 February 2007; received in revised form 13 September 2007; accepted 18 September 2007

Abstract

The first complete cyclic sedimentary successions for the early Paleogene from drilling multiple holes have been retrieved during two ODP expeditions: Leg 198 (Shatsky Rise, NW Pacific Ocean) and Leg 208 (Walvis Ridge, SE Atlantic Ocean). These new records allow us to construct a comprehensive astronomically calibrated stratigraphic framework with an unprecedented accuracy for both the Atlantic and the Pacific Oceans covering the entire Paleocene epoch based on the identification of the stable long-eccentricity cycle (405-kyr). High resolution X-ray fluorescence (XRF) core scanner and non-destructive core logging data from Sites 1209 through 1211 (Leg 198) and Sites 1262, 1267 (Leg 208) are the basis for such a robust chronostratigraphy. Former investigated marine (ODP Sites 1001 and 1051) and land-based (e.g., Zumaia) sections have been integrated as well. The high-fidelity chronology is the prerequisite for deciphering mechanisms in relation to prominent transient climatic events as well as completely new insights into Greenhouse climate variability in the early Paleogene. We demonstrate that the Paleocene epoch covers 24 long eccentricity cycles. We also show that no definite absolute age datums for the K/Pg boundary or the Paleocene–Eocene Thermal Maximum (PETM) can be provided by now, because of still existing uncertainties in orbital solutions and radiometric dating. However, we provide two options for tuning of the Paleocene which are only offset by 405-kyr. Our orbitally calibrated integrated Leg 208 magnetostratigraphy is used to revise the Geomagnetic Polarity Time Scale (GPTS) for Chron C29 to C25. We established a high-resolution calcareous nannofossil biostratigraphy for the South Atlantic which allows a much more detailed relative scaling of stages with biozones. The re-evaluation of the South Atlantic spreading rate model features higher frequent oscillations in spreading rates for magnetochron C28r, C27n, and C26n.

© 2007 Elsevier B.V. All rights reserved.

Keywords: Paleocene; Orbital tuning; Cyclostratigraphy; ODP; Magnetochrons; Biostratigraphy; K/Pg boundary; PETM

1. Introduction

Astronomical tuning resulted in a new generation of geological time scales with unprecedented accuracy, resolution, and stability (Hilgen et al., 2006a). For the

* Corresponding author. Fax: +49 421 218 9865672.

E-mail address: tho@uni-bremen.de (T. Westerhold).

first time the GTS2004 presents an Astronomically Tuned Neogene Time Scale (ATNTS2004, Lourens et al., 2004). In contrast, astronomical calibration of the Geological Time Scale in its older Cenozoic parts is more problematic and requires careful evaluation of uncertainties (Röhl et al., 2001; 2003; Gradstein et al., 2004; Westerhold et al., 2007). With the availability of the new astronomical solutions of Laskar et al. (2004) and Varadi et al. (2003), La2004 and Va2003 hereafter, it is now possible to expand the astronomically tuned timescale into the early Paleogene. Cyclic late Paleogene sediments recovered during Leg 199 and retuning of Shackleton et al.'s (1999, 2000) data to the new La2004 solution provided the first tuned timescale spanning back to the Eocene/Oligocene boundary (Pälike et al., 2004, 2006; Wade and Pälike, 2004; Coxall et al., 2005). A composite depth record from ODP Site 1052 (Leg 171B) provided the basis to extend the astronomically calibrated time scale into the middle Eocene (Pälike et al., 2001). Although strong orbital influence in early Paleogene section has been documented, only floating orbital time scales have been established for early Eocene and Paleocene intervals up to today (Cramer, 2001; Cramer et al., 2003; Röhl et al., 2001, 2003; Dinarès-Turell et al., 2003; Luterbacher et al., 2004; Westerhold et al., 2007).

There is especially a need for a complete astronomically-tuned Paleogene time-scale as observed changes related to palaeoceanographic events in the Paleogene occur significantly faster than the temporal resolution by classical biomagnetostratigraphy can resolve. Up to now the challenge of stitching the patterns documented in published records into a continuous orbital chronology remained (Herbert, 1999). With new records available from ODP Legs 198, 199, 207 and 208 we have entered a new era in the research of early Cenozoic palaeoceanography. Especially the sites from Legs 198 (Shatsky Rise) and Leg 208 (Walvis Ridge) are providing the first complete spliced records for the early Paleogene from drilling multiple holes, as the first depth transects for the early Paleogene for both the Pacific and Atlantic Oceans (Zachos et al., 2004; Bralower et al., 2006). The integration of these records to a robust stratigraphic framework has provided the first accurate duration of magnetochrons C24r and C25n, as well as an evaluation of absolute age estimates for the early Eocene warming events (Paleocene–Eocene Thermal Maximum — PETM, Elmo layer, and “X” event) (Lourens et al., 2005; Röhl et al., 2005; Westerhold et al., 2007). A definite tuning of the 55 Ma old records to the La2004 and Va2003 solutions turned out to be impossible, because the precision of the orbital solution for the time interval older than 42 Ma is limited (Laskar et al., 2004;

Machlus et al., 2004; Westerhold et al., 2007). However, tuning should be viable using the long eccentricity cycle (405-kyr), because of its stability far back in time (Varadi et al., 2003; Laskar et al., 2004), resulting in still floating time scales only. Here, we would like to report on the first complete astronomically calibrated stratigraphic framework for both the Atlantic and the Pacific Ocean covering the entire Paleocene epoch.

2. Material and methods

The continuous record drilled during ODP Legs 198 and 208 provide the basis to construct a complete stratigraphic framework for the Paleocene and to reconstruct the early Cenozoic climate history in detail. For this study we analyzed three cores from ODP Leg 198 (Shatsky Rise, North Pacific; Sites 1209, 1210, and 1211), and two cores from ODP Leg 208 (Walvis Ridge, South Atlantic; Sites 1262 and 1267) (Bralower et al., 2002a; Zachos et al., 2004). In addition, we use published data from the land-based marine section in Zumaia (ten Kate and Sprenger, 1993; Dinarès-Turell et al., 2002; Dinarès-Turell et al., 2003; Bernaola and Mon-echi, 2007) and from marine sections drilled at ODP Site 1001 (Leg 165 — Caribbean Sea, Nicaragua Rise; Röhl et al., 2001), and Site 1051 (Leg 171B — Blake Nose; Cramer et al., 2003; Röhl et al., 2003) (Fig. 1).

2.1. Physical properties and X-ray fluorescence (XRF) scanning

Whole core magnetic susceptibility data (MS) of the multi-sensor track (MS-MST) measurements were routinely measured during Leg 198 (Shipboard Scientific Party, 2002a) and Leg 208 (Shipboard Scientific Party, 2004a). Cyclic variations in these data were successfully used to re-determine depth offsets and revise the shipboard composite sections of Sites 1209, 1210, and 1211 (Westerhold and Röhl, 2006), and served as the primary tool for high-resolution correlation among Leg 208 Sites (Shipboard Scientific Party, 2004b).

X-ray fluorescence (XRF) measurements of iron (Fe) show a significantly higher signal-to-noise ratio, a more consistent hole-to-hole agreement than any of the shipboard physical property measurements (e.g., GRA, color reflectance, MS; Westerhold et al., 2007), and allow the construction of a more accurate high-resolution composite depth scale (Röhl and Abrams, 2000; Evans et al., 2004). Therefore, for this study we analyzed the elemental composition of sediment cores using XRF core scanners of Bremen University (Röhl and Abrams, 2000; Röhl et al., 2000), which allow high-

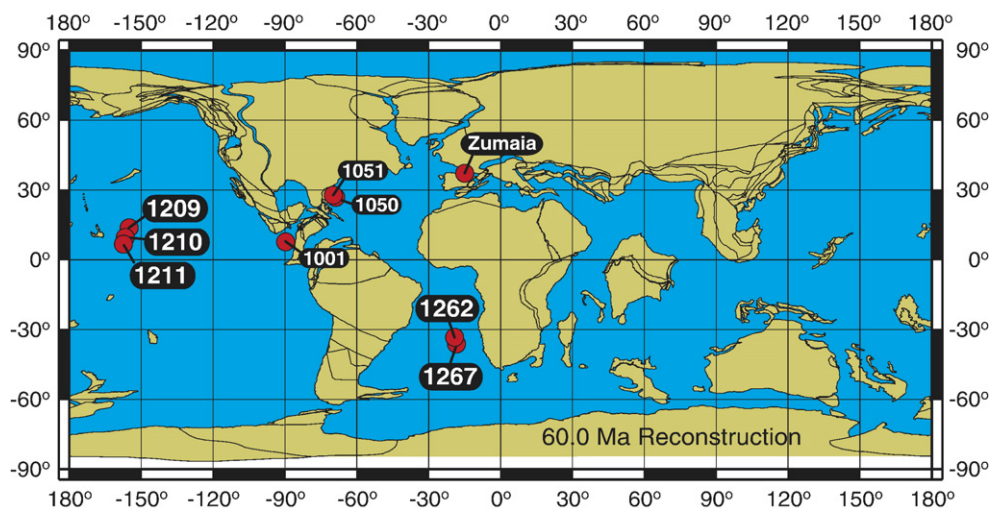


Fig. 1. Paleocene (60.0 Ma) palaeogeographic reconstruction showing the location of the records used in this study. Reconstruction made using the Web-based software at <http://www.odsn.de/odsn/services/paleomap/paleomap.html> (Hay et al., 1999). See color version of this figure in the HTML.

resolution, nearly continuous, non-destructive analyses of major and minor elements at the surface of split cores (Jansen et al., 1998; Richter et al., 2006). XRF data were collected every 2 cm downcore over a 1 cm² area using 30 seconds count time.

2.2. Nannofossil biostratigraphy

At Site 1262 Paleocene calcareous nannofossil biohorizons have been detected in detail in the interval covering magnetochrons C24r through C29r. Datums for the interval C24r–C25n are from Westerhold et al. (2007). Positions of the nannofossil biohorizons in Fig. 2 are based on the new detailed data from Site 1262, whereas the biostratigraphy for Site 1267 is mostly from shipboard data, and was only partially refined. At Site 1262 biohorizons were defined from the distribution ranges of the index species, obtained through semi-quantitative counting of selected taxa, in a set of samples collected with an average spacing of 20 cm. In the interval between the PETM and C27n the considered biohorizons were selected from those described in detail by Agnini et al. (2007). The biohorizons for the K/Pg boundary are from Bernaola and Monechi (2007) while the selected biohorizons in the interval between the top of C27r to C29n are from Monechi and Reale (pers. comm.).

The nannofossil assemblages showed the sequence of evolutionary changes that make up the biostratigraphic framework of the standard Zonations of Martini (1971) and Bukry (1973, 1978), from the K/Pg boundary (base NP1 or CP1) to NP8/NP9 (CP7/CP8) boundary. We use “LO” and “HO” for the biohorizons to denote the lower-

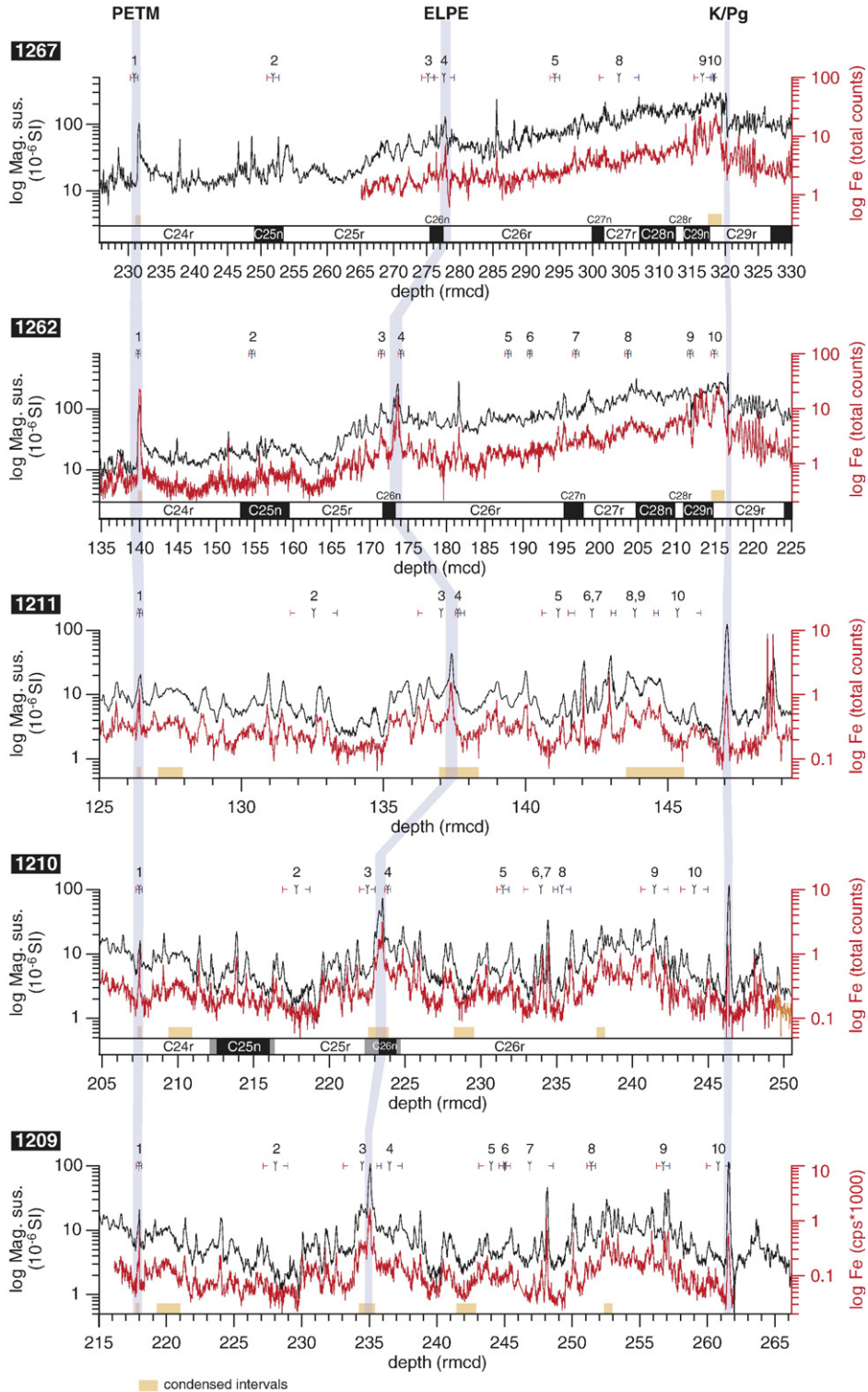
most and highest occurrence of the index species. As suggested by Perch-Nielsen (1985) the *Cruciplacolithus intermedius* (= *Cruciplacolithus tenuis* s.l.) LO and the *Cruciplacolithus edwardsii* (= *Chiasmolithus danicus* s.l.) LO have been utilized as markers of NP2 and NP3 zones respectively. The biohorizons *Ellipsolithus macellus* LO, marker of Zone NP4, and *Heliolithus riedelii* LO, marker of Zone NP8, were considered unreliable and useless for correlation among Walvis Ridge and Shatsky Rise sites. The detected biohorizons, together with a few additional marker events, are summarized in Table S1. Calcareous nannofossil biohorizons for the Paleocene of the Shatsky Rise sites are from Bralower (2005) (see Table S2).

2.3. Magnetostratigraphy

Two types of palaeomagnetic measurements were made on sediments collected during ODP Leg 198; pass-through measurements on half-cores and discrete sample measurements. Discrete sample cubes (2 cm × 2 cm) were collected during Leg 198 to augment measurements using the shipboard pass-through magnetometer. Shipboard measurements on half-cores were made at 5-cm intervals. A total of 2191 discrete samples were taken at 10 to 50-cm intervals. Discrete samples were collected from the center of the half-cores to avoid deformation at the outer edges of the core. Magnetic measurements on the cubes were performed in the magnetically shielded room at the University of Florida (USA) using a 2G Enterprises cryogenic magnetometer. The samples were step-wise alternating-field (AF) demagnetized using a D-Tech D2000 AF demagnetizer.

Magnetization component directions were determined using the method of [Kirschvink \(1980\)](#), applied to the 20- to 60-mT peak field demagnetization interval.

To refine the shipboard magnetostratigraphy of Leg 208 alternating field and thermal demagnetization of discrete samples have been carried out, predominantly



on samples from Sites 1262 and 1267 (Bowles, 2006). This significantly improved the identification of most boundaries in the Paleocene and Upper Cretaceous sections to within 10–30 cm. Detailed correlations between Sites 1262 and 1267 done in this study suggested that the C29r/C29n boundary as picked by Bowles (2006) needs to be revised. Therefore we analyzed additional samples at Sites 1262 ($n=21$) and 1267 ($n=24$) across the C29n/C29r boundary. These additional discrete samples were taken from the working half cores in 8 cm³ cubes. Samples were AF demagnetized in steps (0, 7.5, 10, 15, 20, 25, 30, 35, 40, 50, and 60mT) using a 2G Enterprises cryogenic magnetometer at Bremen University. These samples appear to be especially susceptible to acquisition of a spurious, synthetic remanence during demagnetization; a similar phenomenon was observed in several samples from the C29r/C29n interval by Bowles (2006). For this reason, and for this interval only, we do not use inclination as calculated by principal component analysis. In identifying the C29r/C29n boundary at sites 1262 and 1267 we use the inclination after demagnetization to 20 mT (Table S3). At this level of demagnetization, the drilling remanence is nearly completely removed, and the synthetic remanence remains small. The 20 mT remanence alone should be sufficient for our purposes, because we are primarily interested in polarity and not a precise description of the field direction. For all intervals besides C29r/C29n we use the remanence direction as calculated by principal component analysis (Kirschvink, 1980) for AF steps from 15 to 40 mT (5 to 7 points) for most samples, excluding poorly samples as in Bowles (2006).

3. Results

3.1. XRF data

All five sites include the PETM (Shipboard Scientific Party, 2004b), the Early–Late Paleocene Biotic Event (ELPE) (Bralower et al., 2002b; Röhl et al., 2004; Petrizzo, 2005), and the K/Pg boundary event (Fig. 2). All records exhibit extraordinary and explicit high-frequency cyclicity in the MS data but even more pro-

nounced in the Fe intensity data (Fig. 2). MS and Fe records exhibit very similar patterns (i.e. high MS corresponds to high Fe intensity) because both signals reflect the concentration of iron (oxides) bearing minerals, whereas the high-frequency variability seems less well amplified in the MS data. Due to higher sedimentation rates (1 to 3 cm/kyr) the Walvis Ridge sites exhibit more details in the high-frequency (or precession) band than the Shatsky Rise sites with sedimentation rates of less than 1 cm/kyr. The three most prominent events (K/Pg, ELPE, and PETM) are all characterized by dark red or brown clay-rich layers also reflected by relatively high MS and Fe values (Fig. 2).

The cyclic variations in MS and Fe content as indicated in the core logging and scanning data are interpreted as changes in the amount of clay present in the sediment. These changes appear to be controlled by variations in the amount of dissolution of carbonate as indicated by variations in foraminiferal fragmentation and benthic/planktonic foraminiferal ratios (Zachos et al., 2003; Hancock and Dickens, 2005;). Milancovitch scale variations of the oceanic carbonate ion concentration and thus synchronous changes in the lysocline depth of Pacific as well as Atlantic Ocean might be driven by the expansion and contraction of biosphere productivity in response to changes in solar insolation (Pälike et al., 2006). The sedimentary clay content thus can be interpreted as an inversed indicator for lysocline depth variations generated by the astronomically driven carbon cycle.

3.2. Bio- and magnetostratigraphy

We compiled the available bio- and magnetostratigraphic data for the studied interval of Site 1262. A reliable magnetostratigraphy has been developed for Site 1267 as well (Bowles, 2006). For the Shatsky Rise sites a consistent magnetostratigraphic record could not be acquired because of weak magnetization intensities due to the relatively high carbonate content. The upper Cretaceous and Paleocene through Oligocene sediments at Shatsky Rise are poorly consolidated and thus hamper a well preserved palaeomagnetic signal (Bralower et al.,

Fig. 2. Paleocene composite records of ODP Leg 198 Sites 1209, 1210, 1211, and Leg 208 Sites 1267, 1267 versus meters composite depth (mcd) or revised meters composite depth (rmcd). For all sites MS records are plotted in black and Fe records plotted in red on a logarithmic scale. For Sites 1210, 1262, and 1267 the position of magnetochron boundaries with error ranges are plotted in grey. The arrows with error-bars indicate the position of calcareous nannofossils biohorizons: 1. abundance cross-over *Fasciculithus/Z. bijugatus*, 2. LO *D. multiradiatus*, 3. LO *D. mohleri*, 4. LO *H. kleinpellii*, 5. LO *F. tympaniformis*, 6. LO *Fasciculithus* spp., 7. LO *C. bidens*, 8. LO *T. pertusus*, 9. LO *C. edwardsii* (= *C. danicus*. s.l.), 10. LO *C. intermedius* (= *C. tenuis* s.l.). The three blue lines across the plots mark the position of the Paleocene–Eocene Thermal Maximum (PETM), the Early–late Paleocene Biotic event (ELPE), and the K/Pg boundary. Orange bars mark identified condensed intervals based on detailed Site-to-Site and Leg 198 to Leg 208 correlations. (For interpretation of the references to colour in this figure legend, the reader is referred to the web version of this article.)

2002a; Bralower et al., 2006). Only Chron C25n and C26n could be identified at Site 1210 (Fig. 2). After a site to site correlation (“cycle-to-cycle”) between Leg 198 and Leg 208 records (Table S4, S5), we established a high resolution correlation between the records from the two oceans (Background Fig. F1, Table S6). This way we were able to integrate all stratigraphic information to identify condensed sections (Fig. 2). Based on this correlation and due to their relative completeness we defined Sites 1209 and 1262 as reference sections for the North Pacific and South Atlantic respectively. For the Walvis Ridge Sites the new discrete sample inclinations allow us to improve the Bowles (2006) position of the C29n/C29r boundary at Sites 1262 and 1267 (Fig. 3, Table S7). Because of the need to revise the Paleocene biostratigraphy, we provide the relative position of nannofossil events in C24r to C29r as well as their possible absolute age for Site 1262 (Table S1) and 1209 (Table S2).

4. Cyclostratigraphy

Due to its stability far back in geologic time (Varadi et al., 2003; Laskar et al., 2004) the long-eccentricity cycle will serve as the base for constructing an astronomically calibrated stratigraphic framework for the

Paleocene. In order to extract the long (405-kyr) and short (100-kyr) eccentricity cycles from the sedimentary records we initially followed the approach of Weedon (1993, 2003) and calculated evolutionary spectra in the depth domain to both identify and detect distinct changes in the dominant cycle periods. We used the wavelet analysis method to compute evolutionary spectra. Wavelet software was provided by C. Torrence and G. Compo (<http://paos.colorado.edu/research/wavelets>). Prior to wavelet analysis the data have been detrended and normalized.

Parallel bands in the Wavelet Power Spectra demonstrate that spectral power is located at distinct periods (Figs. F2 and F3). Based on bio- and magnetostratigraphy these bands can be related to long and short eccentricity cycles (e.g., for the Fe data from Site 1262 in Fig. F2 and for stacked MS data from Site 1209 in Fig. F3). The periodicities have a 1:4 frequency ratio, diagnostic for a combination of the long and short eccentricity cycle. Secondly, strong shifts in the spectral bands for both sites suggest changes in cycle periodicities due to changes in sedimentation rates at certain intervals. By far the most dramatic change occurs at the K/Pg boundary at Walvis Ridge, when accumulation rates drop by 75% and therefore spectral power shifts from precession into the eccentricity band (Shipboard

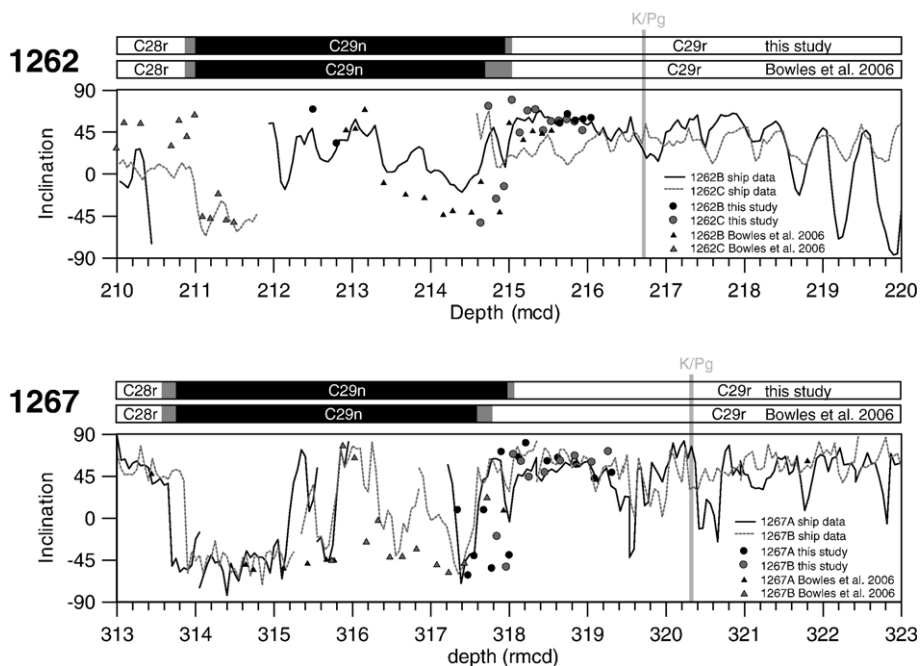


Fig. 3. Magnetostratigraphy of the C29n/C29r boundary for Sites 1262 and 1267. Shipboard pass-through inclination (demagnetized to 15 mT; black and grey-dashed lines) and discrete sample inclination at 20 mT (this study by black and grey circles; Bowles (2006) data by black and grey triangles) are shown. General magnetostratigraphic interpretation is presented at the top; black=normal polarity, white=reverse polarity, grey=indeterminate polarity. K/Pg=Cretaceous/Paleogene boundary.

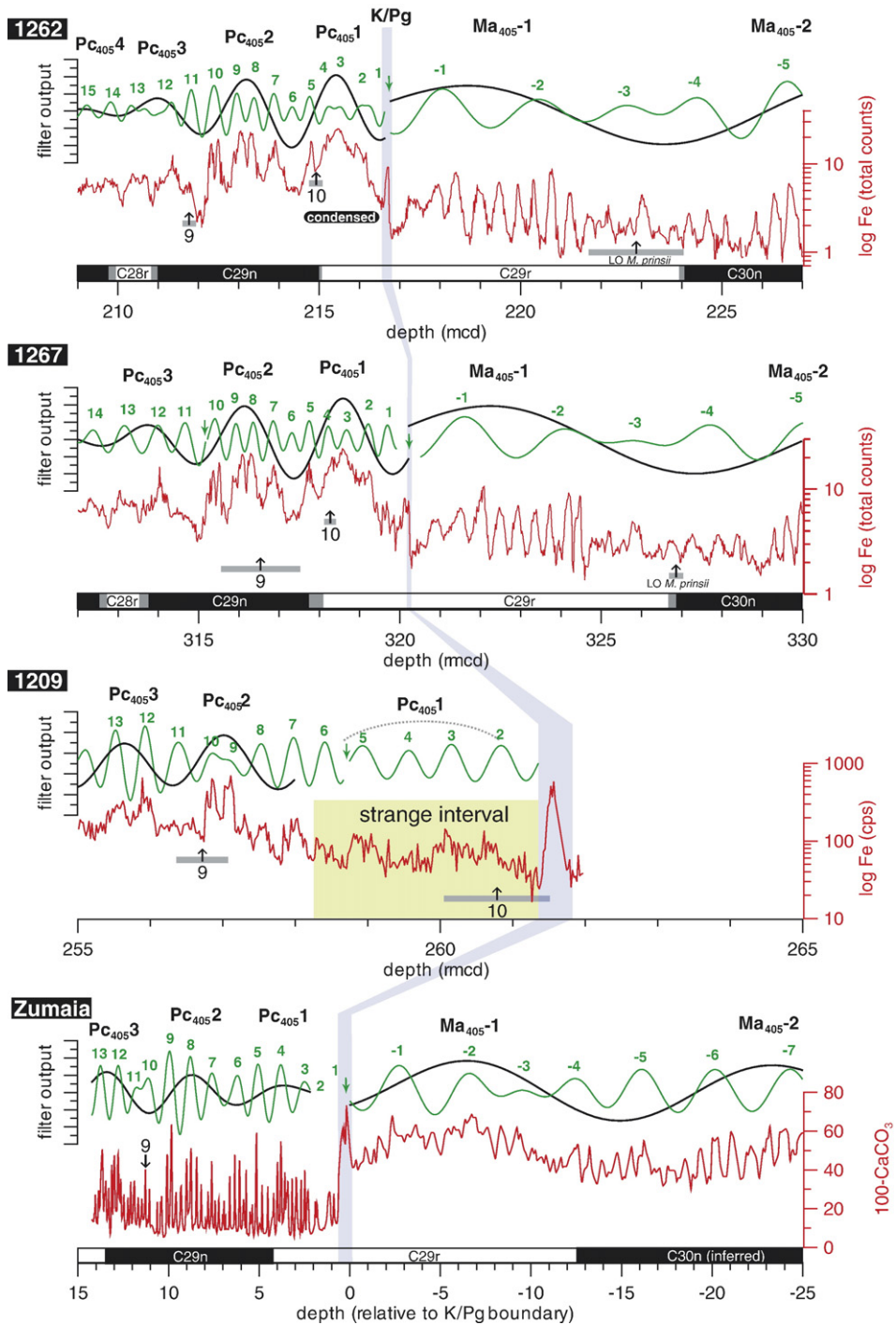


Fig. 4. Cyclostratigraphy across the K/Pg boundary from top of magnetochron C30n to base of magnetochron C28n (Ma₄₀₅₋₂ to Pc₄₀₅₋₄) for sediments from Walvis Ridge, Shatsky Rise, and Zumaia using high-resolution XRF Fe intensity data (1209, 1262, and 1267) and amount of terrigenous material (100 — Carbonate wt.%) (Zumaia; ten Kate and Sprenger, 1993). The position of the K/Pg boundary is indicated (blue line). The short (green) and long (black) eccentricity-related cycles have been extracted by Gaussian filtering. The filters have been adjusted according to the proposed change in cycle thickness by detailed wavelet analysis (for details see supplementary Fig. F2 and F3). Green arrows indicate changes in the width of the applied bandpass filter. The green numbers indicate the short eccentricity (Pc₁₀₀) maxima and the black labels indicate the long eccentricity (Pc₄₀₅) maxima relative to the K/Pg boundary. The arrows with grey error-bars (based on sample interval) indicate the position of calcareous nannofossils biohorizons: 9. *LO C. edwardsii* (= *C. danicus* s.l.), 10. *LO C. intermedius* (= *C. tenuis* s.l.). For further discussion see text. (For interpretation of the references to colour in this figure legend, the reader is referred to the web version of this article.)

Scientific Party, 2004b). The K/Pg boundary is followed by a condensed period of ~400 kyr at Sites 1262 (up to ~214 mcd) and 1267 (up to ~317 rmcd), whereas the record from Site 1267 seems to be less condensed than the 1262 section. At both sites the record slowly recover from this condensed interval into a period of low variability in amplitude from ~212 to ~203 mcd at Site

1262 and ~315 to ~306 rmcd at Site 1267. From here up to the PETM the sediment cycles seem to be stable with just a small shift at the ELPE event (Fig. F2) and at the “post-ELPE-low” (~164 mcd at 1262, ~265 rmcd at 1267). The “post-ELPE-low” is characterized by very low amplitudes in both Fe and MS data. This feature can also be identified in the Shatsky Rise sites (~229 rmcd

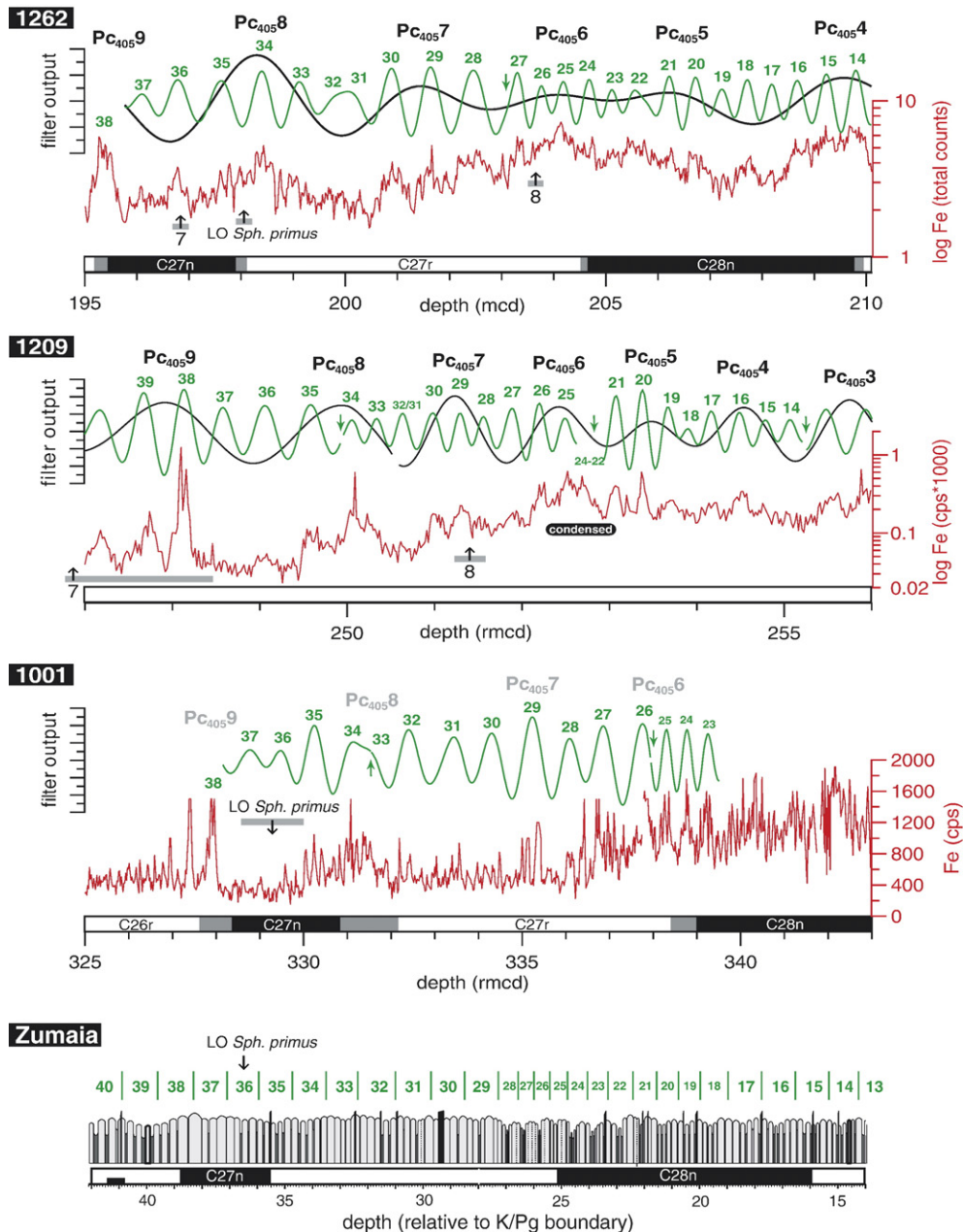


Fig. 5. Fe intensity data and cyclostratigraphy for the intervals of magnetochrons C28n to C27n (Pc₄₀₅4 to Pc₄₀₅9) from Walvis Ridge (1262), Shatsky Rise (1209), Nicaragua Basin (1001), and Zumaia. Data for Site 1001 from (Röhl et al., 2001); log for Zumaia from Dinareš-Turell et al. (2003). For legend of figure see caption of Fig. 4. Calcareous nannofossils biohorizons: 7. LO *C. bidens*, 8. LO *T. pertusus*. Note the strong changes of cycle thickness at Site 1001 as reported by Röhl et al. (2001). For further discussion see text.

at Site 1209, ~219 rmc at Site 1210, ~134 rmc at Site 1211). In general, the Wavelet Power Spectra for the Shatsky Rise sites show higher power in the low frequency range because the lower sedimentation rates tend to amplify low frequency bands (Weedon, 2003). Shifts in spectral bands at Site 1209 occur at the K/Pg boundary (Fig. F3), the Selandian/Thanetian boundary (sensu GTS 2004, at ~250 rmc), the ELPE event, and prior to the PETM. Additional condensed sections at ~242 and ~220 rmc which are more extended in the deeper sites at Shatsky Rise (Fig. 2), the ELPE event, and the PETM are most likely the effect of carbonate dissolution (Bralower et al., 2002b; Petrizzo, 2005; Zachos et al., 2005; Bralower et al., 2006). At both sites the clear recognition of the precession cycle from the K/Pg boundary to the “post-ELPE-low” is suppressed by low sedimentation rates. Thus precession cycle counting in this interval is not possible. Nevertheless, the stable long eccentricity cycle can be extracted from all sites. Short eccentricity cycles can be identified as well and are used to correlate between sites. In order to establish a robust stratigraphy and to cover critical intervals we also included published data from additional sites.

We used direct cycle counting and Gaussian band pass filtering of the data to construct a cyclostratigraphy from the base of C29r (below the K/Pg boundary) up to the PETM (Figs. 4–8). For the band-pass filtering we removed the K/Pg boundary (Fig. 4), ELPE (Fig. 7) and PETM (Fig. 8) data in order to avoid filter disturbance. As a starting point to begin counting short and long eccentricity cycles we used the Fe and MS peak of the K/Pg boundary (Fig. 4). This is reasonable because the K/Pg boundary is the very base of the Paleocene (Agterberg, 2004) and a global event of short duration (Mukhopadhyay et al., 2001). Wade and Pälike (2004) already proposed a new Paleogene cyclostratigraphic nomenclature defining events by 405-kyr cycle numbers. Due to the current discrepancy between astronomical solutions and radiometric dating in the late Paleocene and early Eocene (Westerhold et al., 2007), and the lack of absolute ages as suitable reference points, a naming scheme as proposed by Wade and Pälike (2004) cannot be applied for the Paleocene right now. However, we follow a similar approach and propose a Paleocene stratigraphic nomenclature in relation to the recognition of short and long eccentricity cycles. The cycle count number is defined by the identified maxima in the MS and Fe data corresponding to an eccentricity cycle maximum (see Fig. 4). Based on the detailed site-to-site correlation identical cycle numbers indicate synchrony in time. For counting toward the younger section starting at the K/Pg boundary we as-

signed positive numbers, counting back in time older than the K/Pg boundary we assigned negative numbers. The stable long eccentricity cycles from the K/Pg boundary toward the younger are referred to as Pc₄₀₅1, Pc₄₀₅2, ..., Pc₄₀₅24 (Pc for Paleocene); back in time as Ma₄₀₅-1 and Ma₄₀₅-2 (Ma for Maastricht). The short eccentricity cycles are referred to as Pc₁₀₀1, Pc₁₀₀2, ..., Pc₁₀₀100 upwards, and Ma₁₀₀-1, Ma₁₀₀-2, ..., Ma₁₀₀-6 downwards from the K/Pg boundary. The K/Pg boundary is within cycle Pc₁₀₀1. The position of each designated short eccentricity cycle in each studied section is listed in Background Table S8.

4.1. Cyclostratigraphy from Top C30n to Base C28n (Ma₄₀₅-2 to Pc₄₀₅4)

The integrated cyclostratigraphy from top C30n to base C28n which comprises the K/Pg boundary event shows a pronounced shift in precession cycle thickness in the Walvis Ridge sections (Fig. 4). This is associated with an amplitude increase of low-frequency variations (Fig. F2). The shift has also been identified in the Zumaia section (ten Kate and Sprenger, 1993) as well as in the South Atlantic DSDP Sites 516F, 527, 528, and 529 (Herbert and D’Hondt, 1990; D’Hondt et al., 1996b), and was interpreted as a strong shift in carbonate accumulation due to a decrease in the nannofossil production (e.g. Hsü et al., 1982; Zachos et al., 1989; D’Hondt et al., 1996a). The integration of Site 1262, Site 1267, and the Zumaia section is straight forward in the interval prior to the K/Pg boundary. Correlation between these sections can be achieved even down to the precession scale level. The C30n/C29r reversal in all sections is close to the minimum between Ma₁₀₀-4 and Ma₁₀₀-3. The position of the K/Pg boundary at Sites 1262 and 1267 with respect to the C30n/C29r boundary is consistent with marine succession elsewhere (e.g. Herbert and D’Hondt, 1990). The C29r/C30n boundary itself occurs at each site close to a low variability “node” dictated by the long eccentricity cycle modulation (Herbert, 1999). For the Shatsky Rise sites we could not establish a robust cyclostratigraphy prior to the K/Pg boundary because no clear cyclic signal could be extracted.

In contrast, the cyclostratigraphic interpretation above the K/Pg boundary is rather complex. At the Zumaia section the first 2 m above the K/Pg boundary seem to be problematic if compared to all the other marine sections. This interval has been interpreted to represent one short eccentricity cycle (Dinarès-Turell et al., 2003), which is of abnormal thickness in relation to the cycles below and above. These thick carbonate beds, located in a minimum of the long eccentricity cycle, could be corrupted by the

long-term effect of the K/Pg boundary (Dinarès-Turell et al., 2003). Dinarès-Turell et al. (2003) counted 12 precession cycles from the K/Pg boundary event to the C29r/C29n boundary. Based on the carbonate record of ten Kate and Sprenger (1993) we counted 15 precession cycles assuming that the unusually thick carbonate bed at ~1.5 m above K/Pg indeed represents two precession cycles. Likewise, another unusually thick carbonate bed at ~0.9 m above K/Pg in the Dinarès-Turell et al. (2003) record also consists of two peaks in the carbonate data of ten Kate and Sprenger (1993). Herbert et al. (1995) identified 14.5 ± 2 precession cycles based on integration of South Atlantic chronology and land-based marine sec-

tions (Zumaia, Agost, Rellu). The correlation between Sites 1262 and 1267 reveals 4 short eccentricity cycles between K/Pg and C29r/C29n boundary, and a maximum in the long eccentricity cycle $PC_{405}1$ between $PC_{100}3$ and $PC_{100}4$. The tuned integrated Leg 208 magnetostratigraphy indicates that the C29n base is 368 to 398 kyr (± 20 kyr) above the K/Pg boundary. This comprises of a total of 18 to 19 (± 1) precession cycles for the interval from the K/Pg boundary to the base of C29n. As a result the abnormal thick short eccentricity cycle as interpreted by Dinarès-Turell et al. (2003) actually represents two short eccentricity cycles. An additional feature in the examined records supports this suggestion: if we look at

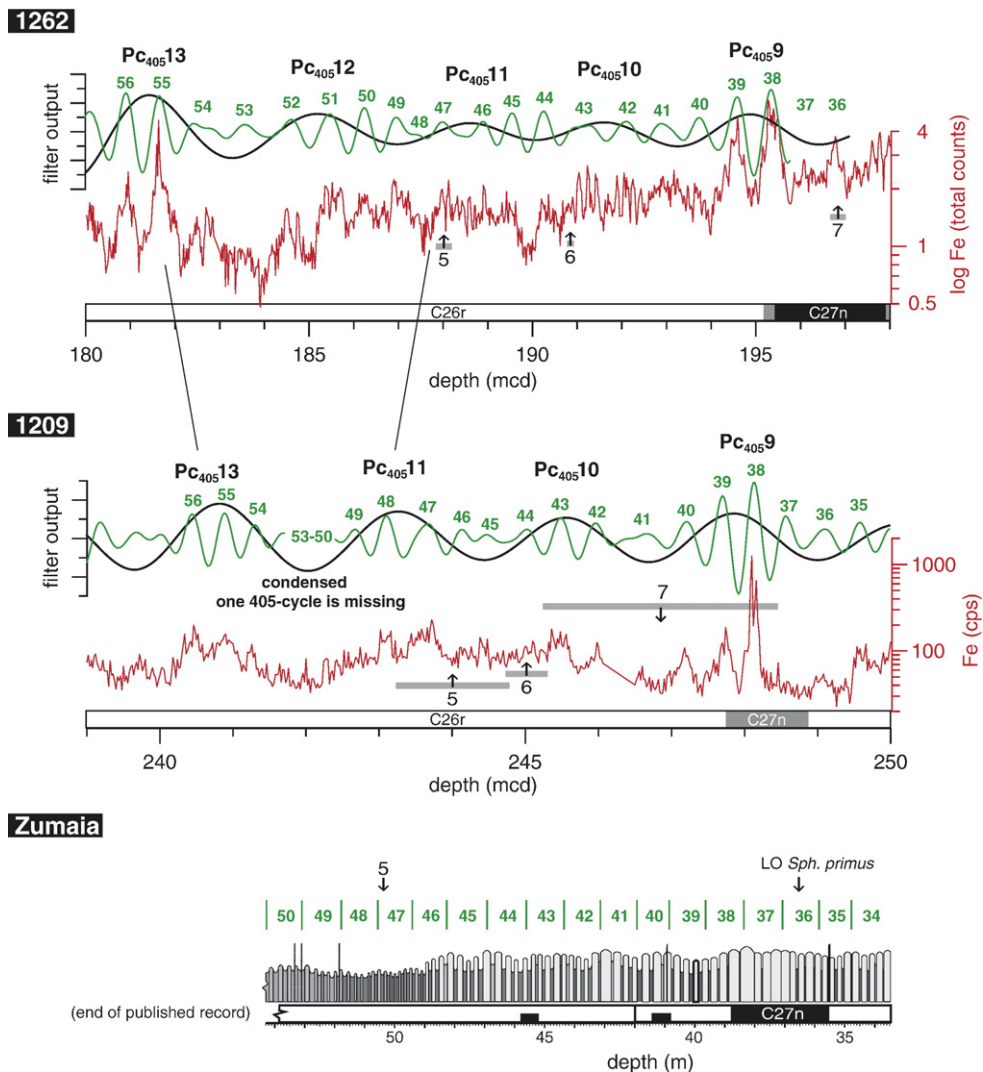


Fig. 6. Fe intensity data and cyclostratigraphy for the magnetochrons C27n to C26r ($PC_{405}9$ to $PC_{405}13$) from Walvis Ridge (1262), Shatsky Rise (1209) and Zumaia (Dinarès-Turell et al., 2003). For legend of figure see caption of Fig. 4. Calcareous nannofossils biohorizons: 5. LO *F. typaniformis*, 6. LO *Fasciculithus* spp., 7. LO *C. bidens*. Note the condensed interval at 1209 which is interpreted to cover one long eccentricity cycle. For further discussion see text.

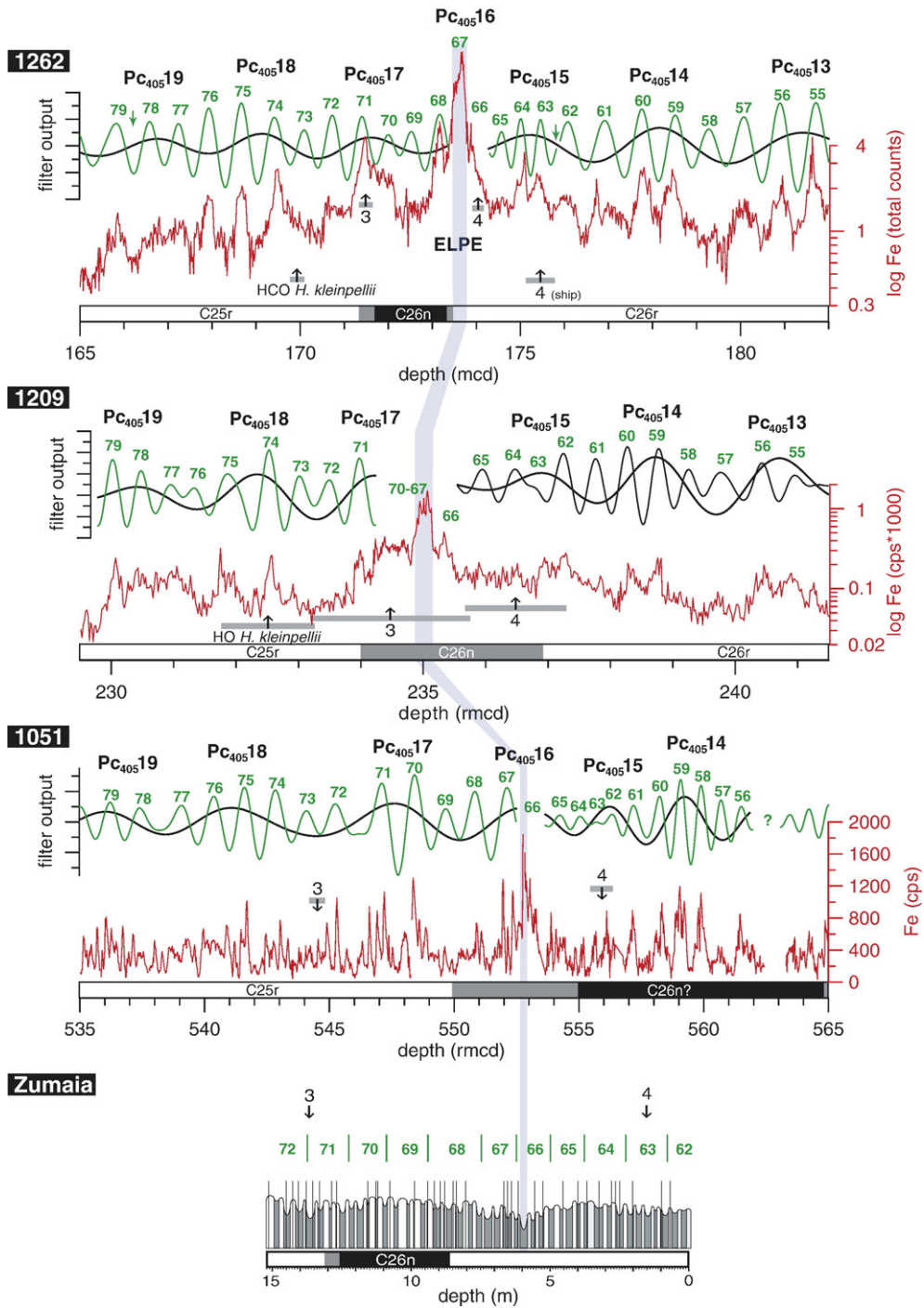


Fig. 7. Fe intensity data and cyclostratigraphy for the magnetochrons C26r to C25r (Pc₄₀₅13 to Pc₄₀₅19) from Walvis Ridge (1262), Shatsky Rise (1209), Blake Nose (1051; Röhl et al., 2003), and Zumaia (Bernaola et al., 2007). Resolution and extent of polarity Zone C26n in 1051 is uncertain. Comparison of Site 1051 to Site 1262 and Zumaia suggests that the C26n interval may be a pervasive overprint at 1051. The position of the ELPE is indicated (blue line). For legend of figure see caption of Fig. 4. Calcareous nannofossils biohorizons: 3. *LO D. mohleri*, 4. *LO H. kleinpellii*. Please note the condensed interval at Shatsky Rise Site 1209 around the ELPE event. For further discussion see text. (For interpretation of the references to colour in this figure legend, the reader is referred to the web version of this article.)

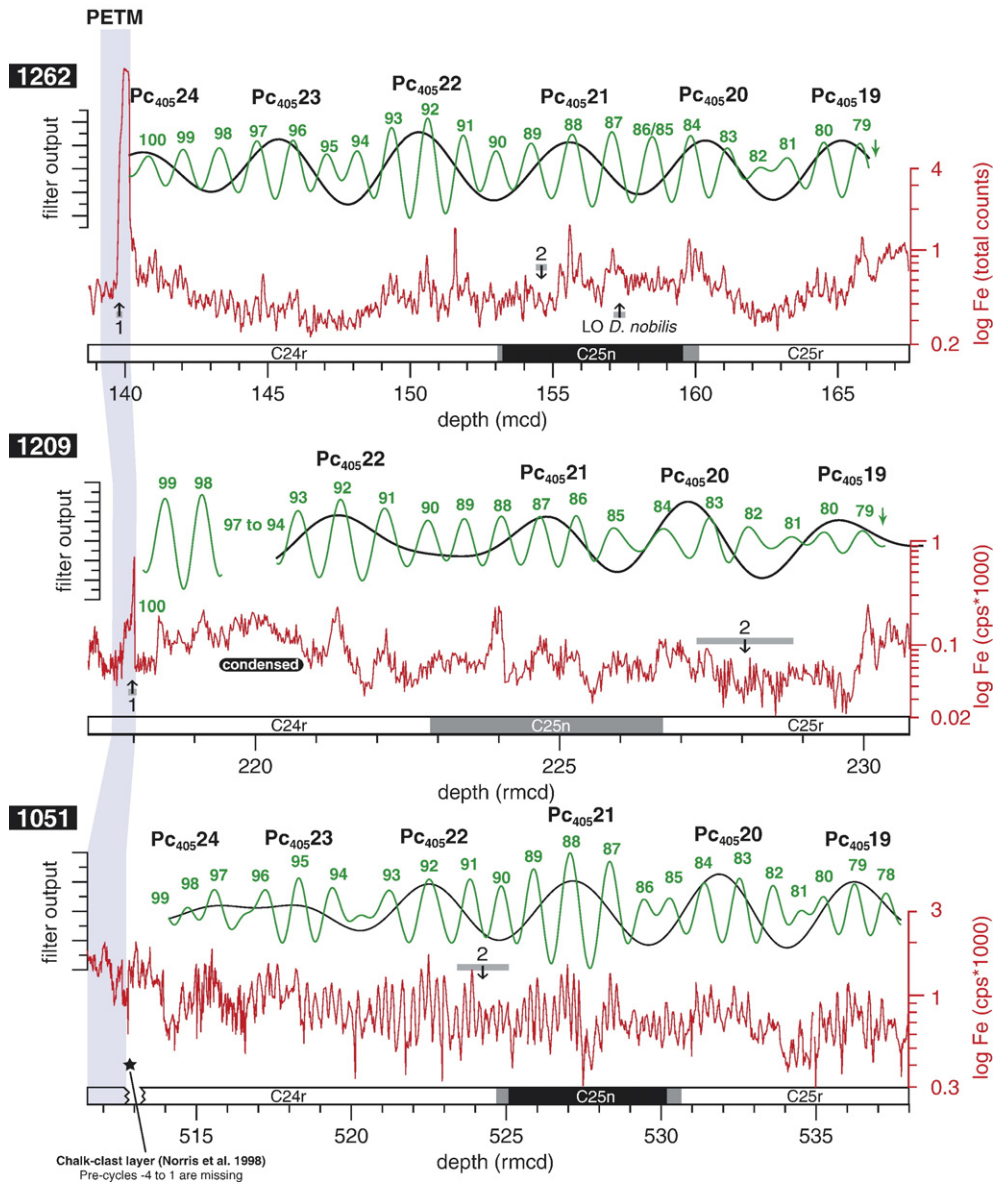


Fig. 8. Fe intensity data and cyclostratigraphy for magnetochrons C25r to C24r ($Pc_{405}19$ to $Pc_{405}24$) from Walvis Ridge (1262), Shatsky Rise (1209), and Blake Nose (1051; Röhl et al., 2003; Ogg and Bardot, 2001). The position of the PETM is indicated (blue line). For legend of figure see caption of Fig. 4. Calcareous nannofossils biohorizons: 1. abundance cross-over *Fasculithus/Z. bijugatus*, 2. LO *D. multiradiatus*. For further discussion see text. (For interpretation of the references to colour in this figure legend, the reader is referred to the web version of this article.)

the eccentricity related amplitude modulation of the precession cycles in Sites 1262, 1267, and the Zumaia record (Fig. 4) one would expect to see two short eccentricity cycles with higher-amplitude to be flanked by two cycles with lower amplitude cycles per 405-kyr cycle. Assuming that $Ma_{100}1$, $Ma_{100}2$, $Pc_{100}3$, and $Pc_{100}4$ are short eccentricity cycles with high-amplitudes centred at 405-kyr maxima two short eccentricity cycles ($Pc_{100}1$, $Pc_{100}2$) should be located in-between. Moreover, when the sedi-

mentary record is tuned to a stable 405-kyr target curve we end up with a phase shift in the 405-kyr filter output applying the estimates of Dinarès-Turell et al. (2003) of just one short eccentricity cycle, which we consider to be unrealistic.

At the North Pacific Shatsky Rise Sites the picture is surprisingly different where more expanded K/Pg boundary layer deposits than in other deep sea records have been found (Bown, 2005; Lees and Bown, 2005; Bralower

et al., 2006). The section represents one of the best-preserved and least-disrupted deep-sea records of this major extinction event (Shipboard Scientific Party, 2002b). Our detailed cyclostratigraphy reveals an expanded interval (labelled “strange interval” in Fig. 4) at the Shatsky Rise site(s). This corresponds to the interval in the South Atlantic Sites 1262 and 1267 with high Fe intensities and accordingly lower carbonate content (Kroon et al., 2007). Although due to the low signal amplitude no clear eccentricity signal can be extracted, the integration of the Walvis Ridge records and the Zumaia section suggests that the interval from the top of the K/Pg layer to the base of Pc₁₀₀₇ spans 5 eccentricity cycles. The decrease in Fe content and thus increase in nannofossil production occurs at cycle Pc₁₀₀₁₁ at Walvis Ridge (Alegret and Thomas, 2007), isochronous to the return or increase of nannofossil abundance at Zumaia (~12 m above the K/Pg boundary; Dinarès-Turell et al., 2003). Slightly enhanced sedimentation rates after the K/Pg boundary at Shatsky Rise lasted for ~800 kyr. This corresponds to relatively high Fe intensities and relatively low carbonate values at Walvis Ridge (<40 wt.%) (Kroon et al., 2007). These results suggest a change in carbonate preservation between Atlantic and Pacific Oceans probably directly linked to the events in relation to and following the K/Pg impact. This difference might be attributed to a decrease in nannofossil production in the Atlantic Ocean (Alegret and Thomas, 2007) and a strong shoaling of the lysocline due to changes in ocean circulation pattern indicated by a shift in deep-water production from the Southern Ocean to the North Pacific at ~65 Ma (Thomas, 2004).

Integrating datasets shows that the base of C29r is located at the top of cycle Ma₁₀₀₋₄, the top of C29r is located at the top of cycle Pc₁₀₀₄, the top of C29n is located at the base of cycle Pc₁₀₀₁₃, and the top of C28r is located in cycle Pc₁₀₀₁₄. The reinterpreted cyclostratigraphy of the Zumaia section (Dinarès-Turell et al., 2003) is presented in the background of Fig. F4.

4.2. Cyclostratigraphy from C28n to C27n (Pc₄₀₅₄ to Pc₄₀₅₉)

We counted ~24 short eccentricity cycles (Pc₁₀₀₁₄ to Pc₁₀₀₃₈) from the base of C28n to the top of C27n at Site 1262 (Fig. 5). Wavelet analysis shows that this interval is characterized by low-amplitude variability and a change from thinner to thicker cycles around cycle Pc₁₀₀₂₆ and Pc₁₀₀₂₇. A similar shift has been observed at ODP Sites 1001 and 1050 (Fig. 5) around the C27r/C28n boundary (Röhl et al., 2001). The Zumaia section reveals a shift towards increasing carbonate bed thickness in this interval (Dinarès-Turell et al., 2003), and

thus also points to a global change in carbonate accumulation at that time. At Shatsky Rise a condensed interval occurred right before cycle Pc₁₀₀₂₆, suggesting that this geochemical reorganization might be linked to changes in deep ocean circulation as indicated by neodymium isotope records at ~63 Ma (Thomas, 2004).

Another critical interval characterized by low amplitude variability in a long eccentricity cycle minimum, and thus undifferentiated filter output, occurs at cycles Pc₁₀₀₃₁ and Pc₁₀₀₃₂ of Site 1262 (Fig. 5). Nevertheless, incorporation of Site 1001 data (Röhl et al., 2001) suggest, that we would expect two short eccentricity cycles in this interval. Integrating all available records suggests that the duration of C27r is ~10 short eccentricity cycles, consistent with the results for the Zumaia section. The base of C28n is located within cycle Pc₁₀₀₁₄, the top of C28n is located in cycle Pc₁₀₀₂₄, the top of C27r is located in cycle Pc₁₀₀₃₅, and the top of C27n is located in cycle Pc₁₀₀₃₈. Cycle Pc₁₀₀₃₈ is characterized by a prominent peak in both Fe and MS data at all Walvis Ridge and Shatsky Rise sites as well as Site 1001 in the Caribbean Sea (Fig. 5). This widespread peak, which we refer to as the “Top Chron C27n Event”, might correspond to an abnormally thick carbonate bed at Zumaia (~38.4 m; Dinarès-Turell et al., 2003).

4.3. Cyclostratigraphy from C27n to C26r (Pc₄₀₅₉ to Pc₄₀₅₁₃)

The cycle identification in the Site 1262 record was straight forward except for cycles Pc₁₀₀₄₈, Pc₁₀₀₅₃, and Pc₁₀₀₅₄ (Fig. 6). But integration of Sites 1267 and 1262 data confirmed the definition of cycle Pc₁₀₀₄₈, and revealed an expanded interval from Pc₁₀₀₅₀ to Pc₁₀₀₅₄ due to higher sedimentation rates. Because this particular interval contains very low Fe intensities with little amplitude modulation by the long eccentricity cycle we suggest that this interval might be corresponding to a very-long eccentricity minimum (Laskar, 1999; Shackleton et al., 1999; Pälike et al., 2004). At Shatsky Rise this section is condensed at Sites 1209 and 1210 (Pc₁₀₀₅₀ to Pc₁₀₀₅₃), and even missing at the deeper Site 1211 (Pc₁₀₀₅₀ to Pc₁₀₀₆₄) (Figs. 2 and F1). Again, these findings suggest a change in the ocean chemistry and/or circulation pattern at that time. Recently, it was proposed to place the Danian/Selandian boundary based on the findings at the Zumaia section near the LO of *F. tympaniformis* which is situated in a prominent red marl interval (also see status on www.stratigraphy.org/gssp.htm; Bernaola et al., 2006). At Site 1262 the LO of *F. tympaniformis* occurs at Pc₁₀₀₄₇ (Fig. 6, 188.03 mcd), right before the onset of the condensed section of

Shatsky Rise. Integration of records from various sections seem to verify that the top of C28n is located between cycle Pc₁₀₀24 and Pc₁₀₀25, the base of C27n is located at the base of cycle Pc₁₀₀35, and the top of C27n is located close to the top of cycle Pc₁₀₀38.

4.4. Cyclostratigraphy from C26r to C25r (Pc₄₀₅13 to Pc₄₀₅19)

From cycle Pc₁₀₀55 to Pc₁₀₀62 short eccentricity cycles can clearly be identified at Site 1262 and correlated to Site 1209 (Fig. 7). At a depth of ~165 mcd in the Site 1262 record the cycle thickness of eccentricity cycles decreases. This is followed by the prominent ELPE event which is characterized by an outstanding peak in Fe intensity in all investigated sites. At Shatsky Rise this clay-rich layer contains common crystals of phillipsite, fish teeth, and phosphatic micromodules which has been attributed to carbonate dissolution, and is accompanied by shift in foraminiferal assemblages (Bralower et al., 2002b, 2006; Hancock and Dickens, 2005; Lees and Bown, 2005). At Walvis Ridge this interval is characterized by similar lithologic composition and planktonic foraminiferal assemblages to the contemporaneous interval at Shatsky Rise (Zachos et al., 2004). High-resolution correlation between Leg 208 and Leg 198 sites demonstrate that sediments at Shatsky Rise are relatively condensed for ~400 kyr from cycle Pc₁₀₀67 to Pc₁₀₀70. Because of the condensed nature of the ELPE event we also integrated data from Site 1051 (Röhl et al., 2003) in order to estimate the duration of this obviously global event. At Site 1051 the ELPE is a prominent event but represented by a relatively small peak. Based on the correlation of the identified cycles at Sites 1051 and 1262 we propose that the ELPE peak at Site 1262 represents the equivalent of one short eccentricity cycle, labeled Pc₁₀₀67. Data from Site 1051 even show that the prominent peak occurs right at the minimum between Pc₁₀₀66 and Pc₁₀₀67 representing only one precession cycle. New data from the Zumaia section reveal that the ELPE (also informally named Mid Paleocene Biotic Event) is located 8 precession cycles below the top of C26r and characterised by a core duration of ~10–11 kyr (Bernaola et al., 2007). In addition, the excellent record from Zumaia confirms the paleomagnetic interpretation for Site 1262 and suggests that the interval interpreted as C26n in Site 1051A might not be very reliable. But comparing the bio-events from Zumaia, Site 1051 and Site 1262 shows a discrepancy for the position of LO *H. kleinpellii* (event 4 in Fig. 7) in relation to the ELPE event. The detailed work on calcareous nannofossils at Site 1262 suggests that

H. kleinpellii evolves from *H. cantabriae* and that gradual modifications between the two can be observed. This means that there is a time in which specimens with transitional morphologic character exist, so one can not be sure if these specimens are *H. cantabriae* or *H. kleinpellii*. Thus the different placement of LO *H. kleinpellii* probably is a taxonomic problem which has to be addressed in the future.

After the ELPE event cycle counting is straight forward up to the so-called “post-ELPE-low” which begins at cycle Pc₁₀₀80 at all investigated sites. Reliable palaeomagnetic data on the position of C26n are only available from Sites 1262 and 1267. According to our cyclostratigraphy base C26n is located at the center of Pc₁₀₀68 and top C26n is located at Pc₁₀₀71, in agreement with recently published data from the Zumaia section (Bernaola et al., 2007).

4.5. Cyclostratigraphy from C25r to C24r (Pc₄₀₅19 to Pc₄₀₅24)

The cyclostratigraphy from cycle Pc₁₀₀79 to Pc₁₀₀101 (PETM) is based on precession-cycle counting at Sites 1262, 1267, and 1051 (Fig. 8) done by Westerhold et al. (2007). We have extracted the short and long eccentricity cycles from the records of these sites and correlated them to Shatsky Rise. The position of C25n at Shatsky Rise (there we have transferred C25n from Sites 1210 to 1209) is consistent with results from Sites 1262 and 1051 (Westerhold et al., 2007). Moreover, all sites show very low amplitude modulation during Pc₁₀₀80, Pc₁₀₀81, and Pc₁₀₀82 at the “post-ELPE-low” suggesting that this might be indeed a very-long eccentricity cycle minimum. At Shatsky Rise sites the interval from Pc₁₀₀94 to Pc₁₀₀97 prior to the PETM is condensed. The position of the onset of the PETM is at the beginning of Pc₁₀₀101 (Westerhold et al., 2007).

4.6. Summary of Paleocene cyclostratigraphy

We counted ~25 long and 104 short eccentricity cycles from the base of C29r to the onset of the PETM. We counted ~24 long and 100 short eccentricity cycles from the K/Pg boundary to the onset of the PETM (24*405 kyr = ~9720 kyr). Hence, the duration of the Paleocene Epoch based on cyclostratigraphy is ~9720 kyr, close to the GTS2004 estimate of 9700 kyr. We think that we have not missed a complete 405-kyr cycle which should show up as a prominent clay layer in the investigated records. We consider the counting error of short eccentricity cycles in the order of one cycle.

5. Discussion

5.1. Astronomical calibration of the Paleocene time scale

5.1.1. Orbital calibration

The major objective of this study is to provide the first complete astronomically calibrated Paleocene time scale. Extending the astronomically calibrated time scale into the early Paleogene is limited due to the uncertainties of astronomical calculations (Laskar et al., 2004), and the large uncertainties in radiometric age constraints for this time interval (Machlus et al., 2004). Recently, the remarkable cyclic sediments recovered during Leg 208 have been used to construct an orbitally calibrated, but still floating time scale covering the Paleocene and earliest Eocene (~58 to ~53.5 Ma) (Westerhold et al., 2007). A definite tuning to the La2004 and Va2003 solutions turned out to be still very complicated, because the precision of the orbital solution for more than 42 Ma ago is limited (Laskar et al., 2004; Machlus et al., 2004). Eccentricity calculations are identical since 25 Ma, very similar since 40 Ma, and due to the imprecise knowledge of the solar oblateness term J_2 (Laskar et al., 2004) they are totally out of phase beyond 42 Ma. Due to the chaotic motion of planets in the inner Solar System an accurate age determination of successive minima in the very long eccentricity cycle used as tie points to define a first order orbitally tuned time scale (e.g. Shackleton et al., 2000; Pälike et al., 2004;) is not possible before ~42 Ma (Westerhold et al., 2007). Moreover, Westerhold et al. (2007) already demonstrated that robust absolute age estimates that are consistent with recalibrated Ar/Ar ages and current orbital solutions cannot be provided. Therefore, a direct anchoring of geological data to current orbital solutions beyond ~42 Ma is impossible at the moment.

However, tuning would be in principle possible for the long eccentricity cycle (405-kyr), because of its stability far back in time (Varadi et al., 2003; Laskar et al., 2004), resulting in still floating time scales only. Hence, we decided to tune the best available record (Site 1262) to the La2004 solution. Tuning was done by assigning ages of short eccentricity maxima to corresponding Pc_{100} peaks in Fe intensity as identified and labelled in the cyclostratigraphy (Fig. 9, Table S8, pointers are given in Table S9). In the future, records can easily be tuned to more accurate orbital solutions by assigning new ages to the Pc_{100} peaks. Based on the findings of Westerhold et al. (2007) we provide the two most favourite sets of tie-points which are offset by ~405 kyr. Option 1 is based on an age of ~55.53 Ma for

the PETM, option 2 assumes an age of ~55.93 Ma for the PETM (Fig. 9). Ages for the onset of the PETM are according to Westerhold et al. (2007).

5.1.2. Results of orbital calibration

Generally the long eccentricity cycle (Fig. 9) filter output of the two options and the La2004 solution are in phase. Looking in detail the filter outputs show small variations which we attribute to irregular features in the data itself and the uncertainty in the amplitude of each individual eccentricity cycle. For example, cycle $Pc_{100}74$ at Sites 1262 and 1267 appears as a relative strong peak, and corresponds to a relatively low short eccentricity maximum. The relatively strong peak in Fe intensity at $Pc_{100}74$ shifts the maximum of the filter output to older ages suggesting a misfit in the long eccentricity cycle. Based on our integrated stratigraphy $Pc_{100}74$ can not be moved into eccentricity cycle 75 because this would result in inconsistent filter outputs for the entire C25r and C26n interval. The suggestion that the pattern of the data affected the filter output is supported by the comparison of the filter outputs of Sites 1262 and 1267. As shown in Fig. 9, the long eccentricity cycle filter output of Site 1267 Fe intensity in the interval from $Pc_{405}3$ to $Pc_{405}6$ is out of phase if compared to Site 1262 and La2004. Zooming into this interval shows that the pattern for Site 1267 is driven by a condensed section in $Pc_{405}6$. At the top of the condensed section relatively high Fe intensities appear. This may correlate to the Fe peak at cycle $Pc_{100}25$ in Site 1262. However, the different shape in the 1267 data resulted into a shift in the long eccentricity filter output.

5.1.3. Sedimentation rates

At Site 1262 the observed changes in cycle thickness result in changes in sedimentation rates (Fig. 10), supporting proposed environmental changes in the South Atlantic at that time. Again, the most prominent feature of course is the shift at the K/Pg boundary, which is in the order of a magnitude larger than other shifts observed in the record. Sedimentation rates drop from ~2 cm/kyr to ~0.5 cm/kyr across the K/Pg boundary at Site 1262, and from ~4 cm/kyr to ~1 cm/kyr at Zumaia. The Pacific Ocean was less affected by the geochemical reorganization of the global oceans after the K/Pg impact indicated relatively good carbonate preservation for ~800 kyr compared to the Atlantic. In the first 400 kyr after the K/Pg impact the geochemical reorganization was much stronger characterized by the condensed section at Walvis Ridge. The different magnitude of changes in the calcium carbonate preservation in the Atlantic and Pacific Ocean might be related to

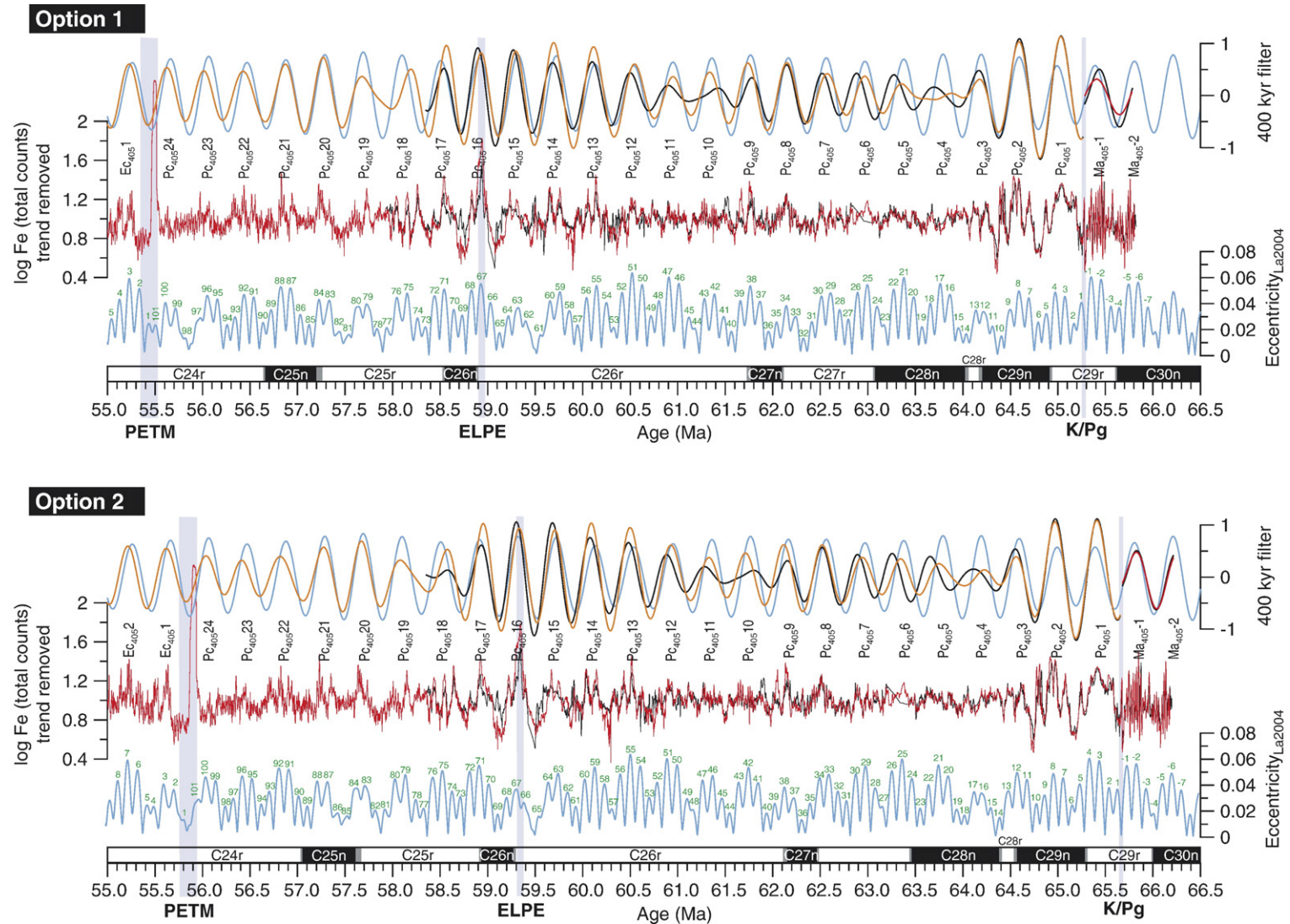


Fig. 9. Two options for the astronomical calibration of detrended Fe intensity data of Sites 1262 (red) and 1267 (black) with the La2004 eccentricity solution (blue) for the entire Paleocene. Both options are offset by one long eccentricity cycle. The green numbers on the eccentricity curves represent the proposed correlation to the P_{100} cycles extracted from the studied records. Bandpass filters for eccentricity (blue), 1262 Fe data (red), and 1267 Fe data (black) were calculated for the 405-kyr long eccentricity component (0.002469 ± 0.0007 cycle/kyr). The naming scheme based on the long eccentricity cycle for the cyclostratigraphic framework is given as described in the text. Positions of the K/Pg boundary, ELPE, and PETM (P/E boundary) are marked by blue lines, and the integrated Walvis Ridge magnetostratigraphy (see text) is plotted. (For interpretation of the references to colour in this figure legend, the reader is referred to the web version of this article.)

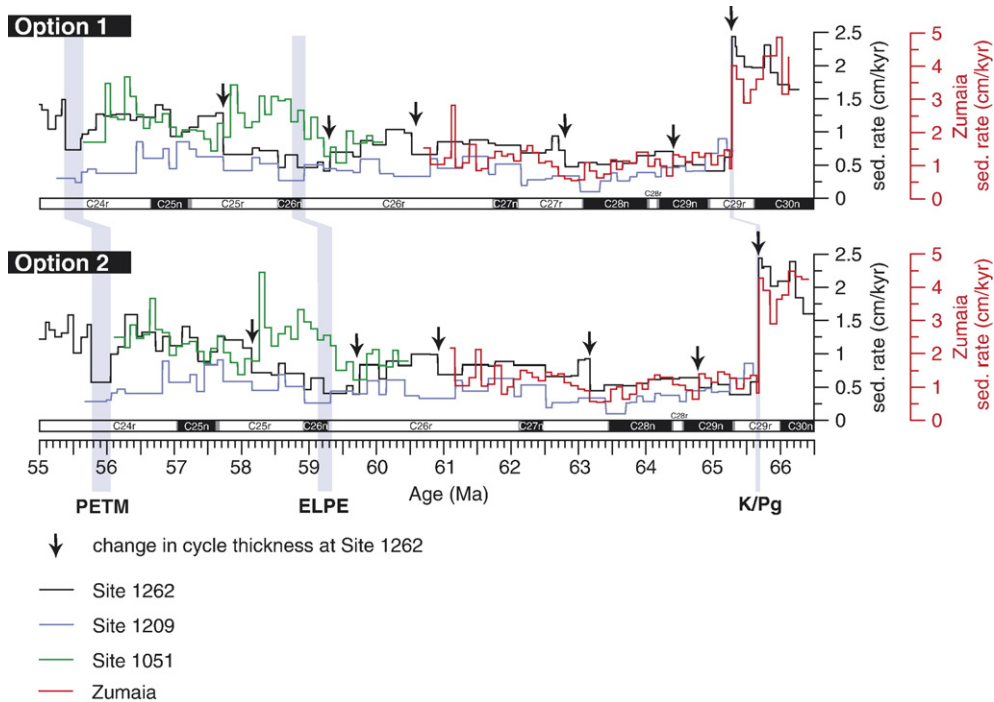


Fig. 10. Resulting sedimentation rate in cm/kyr derived from the orbitally calibrated records from Walvis Ridge (1262, black), Shatsky Rise (1209, blue), Blake Nose (1051, green), and Zumaia (red) plotted against age and integrated Walvis Ridge magnetostratigraphy for both calibration options. Black arrow mark observed changes in cycle thickness at Site 1262. Blue lines mark the K/Pg boundary, ELPE, and PETM. For further discussion see text. (For interpretation of the references to colour in this figure legend, the reader is referred to the web version of this article.)

dramatic modifications in the carbonate production, carbonate production pattern, and ocean circulation after the K/Pg impact (Herbert et al., 1995; Thomas, 2004, Alegret and Thomas, 2007).

Walvis Ridge and Shatsky Rise sites show similar trends in sedimentation rates (Fig. 10) with low rates from K/Pg to ~63 Ma, increased values from ~63 to ~59.5 Ma, lowered values around the ELPE event from ~59.5 to ~58 Ma, and increased values after ~58 Ma (“post ELPE low” Event). The PETM, as an exception from this trend, exhibits lower sedimentation rates due to carbonate dissolution (Zachos et al., 2003, 2005). The observed trends in global sedimentation rate might be related to changes in productivity and/or preservation. Condensed sections have sedimentation rates below 0.5 cm/kyr at Site 1262 and below 0.25 cm/kyr at Site 1209. Interestingly, the lower sedimentation rates from ~59.5 to ~58 Ma are accompanied by higher rates at the shallower Atlantic Site 1051 in this interval (Fig. 10). However, if we consider the condensed sections at Shatsky Rise at this interval, we propose a strong shoaling of the lysocline in the Pacific and Atlantic Ocean around the ELPE event. The ELPE itself is characterized by a strong shoaling of the lysocline and carbonate compensation depth (Petrizzo, 2005).

5.2. Absolute ages for the PETM and K/Pg boundary

Based on cyclostratigraphy the K/Pg boundary and the onset of the PETM are exactly twenty-four (24) 405-kyr cycles apart, ~9720 kyr. According to the two tuning options the distance K/Pg to onset PETM is 9750 ± 10 kyr. For the moment, at least two different absolute ages for the onset of the PETM have to be considered (Westerhold et al., 2007): ~55.53 Ma or ~55.93 Ma. If we add the estimated amount of 9750 kyr we come up with an age of ~65.28 Ma or ~65.68 Ma for the K/Pg boundary (Table 1), respectively. It is important to note that due to the integration of the cycle pattern into the stratigraphic framework the ages of the K/Pg boundary and PETM can only be moved by 405-kyr steps. For example, a third option could be at ~56.33 Ma for the PETM and at ~66.08 Ma for the K/Pg, one long eccentricity cycle older than option two (Table 1).

Radiometric ages are linked to the magnetostratigraphy scale and directly calibrate the Paleogene time scale (Agterberg, 2004). A revised age estimate for the K/Pg boundary of 65.51 ± 0.1 Ma has been obtained by normalizing published radiometric ages for the boundary to a standard monitor age of 28.02 Ma for the Fish

Table 1

Possible absolute ages for PETM and K/Pg boundary. Please note that accurate absolute ages cannot be provided by now (see discussion in the text)

Event	BKSA	GTS2004	Recalibrated	Recalibrated	Recalibrated	This study	This study	This study
	1995		FCT ^a	Ash A1 ^b	Sanadine ^c	Option 1	Option 2	Option 3
P/E boundary (PETM)	55.0	55.00	~55.75	~55.59	(~55.7)	~55.53	~55.93	~56.33
K/Pg boundary	65.0	65.50	~66.65	~65.84±0.04	~65.8	~65.28	~65.68	~66.08
FCT standard age at	27.84	28.02	~28.21	28.12±0.05	28.2 ^d	–	–	–

^a Kuiper et al. 2004, 2005.

^b Swisher et al. (EGU2006).

^c Hilgen et al. (EGU2006).

^d Mean of 28.23 Ma Amsterdam and 28.18 Ma Berkley.

Canyon Tuff (FCT) and 28.32 Ma for the Taylor Creek Rhyolite (TC) (Hicks et al., 2002). Current variations in the absolute age of ⁴⁰Ar/³⁹Ar dating standards are between 1 and 3 percent (Swisher et al., 2006). Thus the ±0.1 Ma uncertainty is probably too low because external uncertainties associated with ⁴⁰Ar/³⁹Ar ages were not considered (for discussion see (Agterberg, 2004)). The full error propagation in Ar/Ar geochronology (e.g. Renne et al., 1998; Min et al., 2000) gives an uncertainty of about 2.5% which is one order higher than the analytical error that is usually indicated. In the Geological Time Scale 2004 the ±0.1 Ma uncertainty was replaced (GTS2004) by a ±0.3 Ma uncertainty for the K/Pg boundary (65.5±0.3 Ma) (Agterberg, 2004; Luterbacher et al., 2004). More importantly, the new GPTS2004 (Ogg and Smith, 2004) utilizes radiometric calibration points calibrated to the FCT age of 28.02 Ma as recommended by Villeneuve (2004). But following recent suggestions by Kuiper et al. (2004, 2005) to use an older age of 28.21±0.04 Ma for the FCT, the age of the K/Pg boundary will become ~0.7% older (~66.05 Ma). Recently, new intercalibrated Ar/Ar ages proposed an age for the K/Pg boundary of ~65.8 Ma (Hilgen et al., 2006b; Swisher et al., 2006).

If we consider a slightly older age than 65.5 Ma for the K/Pg boundary our absolute age from the second solution of ~65.68 Ma and the possible third solution of ~66.08 Ma would be close to the recent recalibrated radiometric estimates. The small difference in ages between Ar/Ar dating and tuning is well within the uncertainty of radiometric dating. Fortunately, because of our stratigraphic framework we now can also look at the age of the PETM and see what happens to this estimate with respect to the different options mentioned above. If we consider option 2 to be correct, the age of the PETM will be ~55.93 Ma. If we consider option 3 to be correct, the age of the PETM will be ~56.33 Ma. Unfortunately, there are no direct radiometric dates available for the PETM up to today. Age estimates are based on interpolation of the relative position of the

PETM and radiometric dated ash layers within magnetostratigraphic C24r (for discussion see Westerhold et al., 2007). If we recalibrate Ar/Ar ages following the suggestion of Kuiper et al. (2004; 2005), Hilgen et al. (2006b), and Swisher et al. (2006), and recalculate the position of the PETM in C24r according to Westerhold et al. (2007) we obtain a radiometric calibrated age of ~55.8 Ma for the PETM. Looking at both PETM and K/Pg ages this simply means that option 1 is too young and option 3 is too old with respect to radiometric dates. However, based on the rather liberal ±0.3 Ma uncertainty in Ar/Ar dating given in the GPTS2004 the range of the absolute age of the K/Pg boundary and the PETM should be 65.50 to 66.10 Ma and 55.50 to 56.10 Ma, respectively. Assuming that the correct absolute ages should be within these boundaries, option 3 has to be rejected. Thus we are left with option 1 and 2. But which one is correct? Due to the uncertainty in the La2004 solution for eccentricity a direct anchoring of the Paleocene cyclostratigraphic framework is not possible (Westerhold et al., 2007). It even gets more complicated considering that U–Pb and ²⁰⁷Pb/²⁰⁶Pb dates are systematically older than ⁴⁰Ar/³⁹Ar by <1% (for discussion see Schoene et al., 2006). This suggests that the recalibrated Ar/Ar ages would be too young and the absolute age of the K/T boundary ~66.10 Ma bringing back option number 3. Unfortunately, because of the relatively large errors in radiometric dating it is still impossible to verify if U–Pb dates are systematically <1% older than ⁴⁰Ar/³⁹Ar (Schoene and Bowring, 2006; Schoene et al., 2006).

All of this leaves us in a dating dilemma which can not be solved right now. Nevertheless, definite absolute ages will be achievable when a new orbital solution which is stable beyond 50 Ma is available, when the Ar/Ar dating technique is more accurate, and when a cyclostratigraphic framework for the entire Paleogene has been developed. Therefore we decided to provide two options (1 and 2) for the absolute ages of events, bio- and magnetostratigraphic boundaries. Based on the

Table 2
Cycle-tuned estimates for the duration of Paleocene magnetochrons

Chron	CK95	GPTS2004	Zumaia	Bjala ^a cycle counting	Herbert et al. (1995)	Röhl et al. (2003)	This study	
	Duration (kyr)	Duration (kyr)	Duration (kyr)	Duration (kyr)	Duration (kyr)	Duration (kyr)	Option 1	Option 2
C24r	2557	2858				2877	3130 (±48)	3149 (±48)
C25n	487	515	441–483 ^b			525	537 (±46)	557 (±43)
C25r	1163	1199				1066	1354 (±51)	1323 (±48)
C26n	357	359					327 (±11)	338 (±12)
C26r	3009	2913				3608	2896 (±31)	2881 (±32)
C27n	356	333	231 (273) ^c	210			324 (±25)	314 (±25)
C27r	1223	1121	1050 (964) ^c	924			980 (±5)	995 (±5)
C28n	1135	1024	1029 (1089) ^c	1113			949 (±17)	923 (±18)
C28r	342	304	252–273 (210) ^c	189			177 (±27)	187 (±29)
C29n	769	685	796–819 (879) ^c	651	672 (±42)		707 (±29)	710 (±32)
C29r	833	743			693 (±63)		713 (±16)	725 (±16)

^a Preissinger et al., 2002.

^b Dinares-Turell, 2002.

^c Dinares-Turell, 2003.

fact that radiometric ages tend to shift to older ages due to the recalibration of the monitor standards we would favour solution 2 to give the correct absolute age estimates.

5.3. Duration of Paleocene polarity chrons: implications for sea-floor spreading-rates

5.3.1. Estimated duration of polarity chrons C29 to C25

The orbitally calibrated high-resolution palaeomagnetic stratigraphy from Leg 208 Sites 1262 and 1267 as well as the re-interpreted Zumaia record also enabled us to revise the Paleocene magnetostratigraphy. As already discussed we provide both the duration (Table 2) and the absolute ages (Table 3) for magnetochrons C29r through C25n for the alternative options 1 and 2. In order to minimize the error bar of the reversal positions, we have integrated the palaeomagnetic data for Sites 1262 and 1267 based on the high resolution correlation. In the following we will refer to the new combined palaeomagnetic stratigraphy as the integrated Leg 208 magnetostratigraphy. The integrated magnetostratigraphy reveals that the main uncertainty for the duration and absolute ages is determined by the uncertainty in the location of the chron boundaries.

The duration of Paleocene magnetochrons for the two provided options roughly agree with the durations as presented in the GPTS2004 (Ogg and Smith, 2004), but zooming into the details exhibit differences. According to our results Chron C25 (Table 2) is ~180 kyr longer than the GPTS2004 estimate. Because the duration of C25n is consistent between our new data and the

GPTS2004, the difference for the total C25 derives from the ~150 kyr longer duration of C25r. The GPTS2004 estimate is based on the minimum duration approximations from Site 1051 (Röhl et al., 2003) which is at that depths based on data from a single drilled hole only. Uncertainty in the exact extent of coring gaps will complicate the duration estimate and thus promote the underestimation of magnetochrons as shown for Chron C24r (Westerhold et al., 2007). Moreover, the C25r/C26n boundary as well as Chron C26n itself are not well defined in Site 1051.

Table 3

Estimates of absolute age of magnetochrons and global events. Please note that accurate absolute ages cannot be provided by now (see discussion in the text)

Chron, Event	CK95	GPTS 2004	Leg 208 integrated	
	Age (ka)	Age (ka)	Option 1	Option 2
			Age (ka)	Age (ka)
PETM [†]	55,000	55,800	55,530 (±10)	55,930 (±10)
C25n (y)	55,904	56,665	56,660 (±1)	57,055 (±1)
C25n (o)	56,391	57,180	57,197 (±46)	57,612 (±43)
C26n (y)	57,554	58,379	58,551 (±5)	58,935 (±5)
C26n (o)	57,911	58,737	58,878 (±6)	59,273 (±7)
C27n (y)	60,920	61,650	61,774 (±25)	62,154 (±25)
C27n (o)	61,276	61,983	62,098 (±1)	62,468 (±1)
C28n (y)	62,499	63,104	63,079 (±4)	63,463 (±5)
C28n (o)	63,634	64,128	64,028 (±13)	64,385 (±13)
C29n (y)	63,976	64,432	64,205 (±14)	64,572 (±16)
C29n (o)	64,745	65,118	64,912 (±15)	65,282 (±16)
K/Pg	65,000	65,500	65,280 (±10)	65,680 (±10)
C30n (y)	65,578	65,861	65,625 (±1)	66,007 (±1)

[†]Onset of carbon excursion.

(y) younger; (o) older.

The duration of Chron C26 is consistent between GPTS2004 and the Leg 208 record, but ~ 400 kyr shorter than from Site 1051 (Röhl et al., 2003) (Table 2). The longer estimate for Site 1051 is probably due to large uncertainties in the exact position of polarity chron boundaries. Chron C26n could hardly been identified in any record in the past. The lack of complete C26n intervals in deep-sea records might be related to the proximity to the ELPE event, which is a time period characterized by wide spread condensation (Röhl et al., 2004; Bralower et al., 2006). Because of the high quality of the palaeomagnetic signal in Leg 208 sediments we consider the estimate for C26 to be the best current available.

The duration of Chron C27 is ~ 150 kyr shorter than in the GPTS2004 and the cyclostratigraphic estimate of Röhl et al. (2001), but consistent with estimates from the land-based marine section in Zumaia (Dinarès-Turell et al., 2003). The incorporation of Sites 1001 and 1050 data (Röhl et al. (2001)) into our stratigraphic framework (Fig. 5) suggests a duration of ~ 1300 kyr for C27, although the error in the polarity reversal position at both sites is too large to provide an estimate as precise as derived from the Leg 208 record.

Our results suggest that C28 is ~ 200 kyr shorter than in GPTS2004 and in the Zumaia section (Dinarès-Turell et al., 2003) (Table 3). The approximate duration of C28 in GPTS2004 is based on interpolation by applying an intermediate spreading rate between C29 and C27 (Röhl et al., 2001; Ogg and Smith, 2004). In contrast, our reinterpretation of the cyclostratigraphy of the Zumaia record across C28 is almost consistent with the Leg 208 duration of ~ 1120 kyr. The biggest difference can be observed at C28r, which is ~ 120 kyr or 40% (!) shorter than in GPTS2004. Our estimate of $\sim 180 \pm 28$ kyr is close to the tuned C28r Chron at Zumaia (~ 210 kyr) (Dinarès-Turell et al., 2003) and the cycle counting at Bjala (Bulgaria, ~ 190 kyr; (Preissinger et al., 2002)). This relatively short estimate has consequences for calculating spreading rates.

Finally, the duration of Chron C29 is close to the GPTS2004 estimate, which for this interval is based on the detailed cyclostratigraphy of Herbert et al. (1995). The retuned Zumaia record is ~ 50 kyr longer in duration which might be due to the uncertainty in the exact position of the reversal at Zumaia and/or the deep marine successions. Following the system of Hallam et al. (1985) and the recommendation of Cande and Kent (1992) to use an inverted stratigraphic placement relative to the present the relative position of the K/Pg boundary within C29r is C29r.514 (option 1) or C29r.547 (option 2). This confirms that the K/Pg

boundary occurred very close the middle of the reversed polarity interval.

5.3.2. Implications for the South Atlantic spreading-rate model

Age and duration of polarity chrons in the standard Geomagnetic Polarity Time Scale (GPTS) are computed by fitting a natural cubic spline to selected calibration ages applied to the widths of magnetic anomalies in the synthetic South Atlantic anomaly profile (Cande and Kent, 1992; Cande and Kent, 1995) (“CK95”). The “CK95” marine anomaly pattern has been recalibrated using an array of astronomical tuning and a suite of additional or revised radiometric age calibrations to C-sequence polarity chrons for the GPTS2004 (Agerberg, 2004; Ogg and Smith, 2004). The calibration of the Paleogene part of the GPTS2004 largely depends on radio-isotopic (e.g., $^{40}\text{Ar}/^{39}\text{Ar}$) dates and cyclostratigraphy (Luterbacher et al., 2004). Due to the large uncertainties in radiometric age constraints and the selection of tie points itself, different versions of the GPTS are indeed possible (Machlus et al., 2004). Our astronomically calibrated integrated Leg 208 stratigraphy provides very accurate estimates of the relative duration of magneto-chrons for the Paleocene epoch. The results show that the GPTS2004 estimates for magneto-chron durations are indeed more accurate than the Cande and Kent (1995) GPTS. The relative age calibration of polarity reversals yield average spreading rates for the synthetic South Atlantic magnetic anomaly profile (Cande and Kent, 1992). In the GPTS2004 spreading rates along the synthetic South Atlantic profile decelerate smoothly through the Maastrichtian to Danian (Fig. 8) to reach a minimum of ~ 13 km/myr at about 55 Ma (Röhl et al., 2001), which sustained in the same order throughout the late Paleocene and early Eocene (60–50 Ma) before spreading rates accelerated again through the middle Eocene. This general trend was identified by CK95 (Cande and Kent, 1995), but a revised curve yielded younger ages for the main deceleration in the Paleocene (Röhl et al., 2001).

With the new integrated stratigraphic framework we can reassess the Paleocene portion of the South Atlantic spreading rate model. Obviously, there is more variability in the spreading rates than can be deduced from the GPTS2004 (Fig. 11). The major deceleration seem to have taken place around Chron C27n (~ 62 Ma) close to the proposed new Danian/Selandian boundary (*F. tympaniformis*; Bernaola et al., 2006) from ~ 17 to ~ 14 km/myr on average, which can also be observed at the Zumaia section. This major change in spreading rate is synchronous with the beginning of volcanism at the

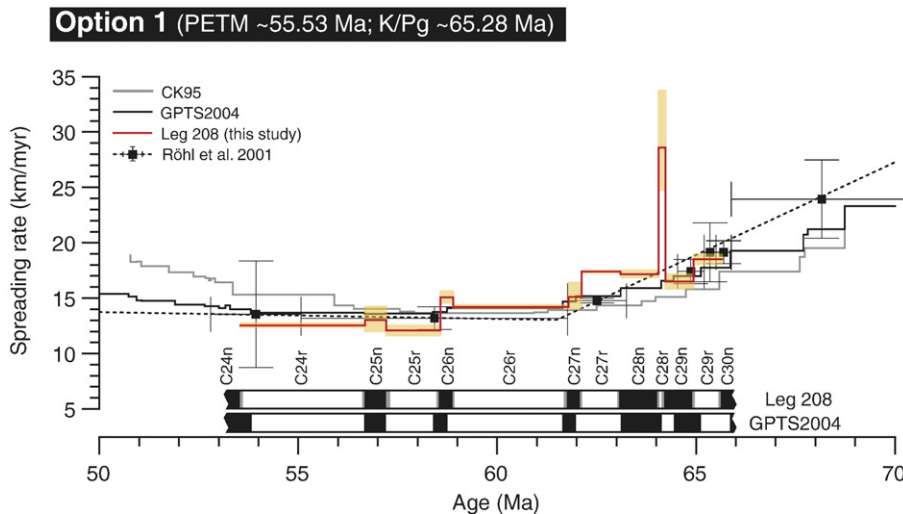


Fig. 11. Revised spreading rates for the synthetic South Atlantic profile of Cande and Kent (1992) based on the new orbital calibration of magnetic polarity chrons C29r to C24r from Leg 208 (Walvis Ridge). Here we show the results from option 1 with PETM at 55.53 Ma and K/Pg at 65.28 Ma. The results for options 2 and 3 are nearly identical with option 1 but offset by 405 and 810 kyr to the older. The spreading rate estimates based on CK95 (Cande and Kent, 1995), GPTS2004 (Ogg and Smith, 2004), and a revised spreading model of Röhl et al. (2001) are also shown. The shaded area around the Leg 208 estimate indicate the error range of spreading rates based on the error in the exact determination of polarity reversal positions in the ODP cores. Note, that higher amplitude oscillation in the spreading rates at the Leg 208 estimates are probably an artifact of the combination of relatively short cycle-tuned polarity chrons and uncertainties in the corresponding magnetic anomaly widths in the South Atlantic synthesis profile (especially for C28r).

southeast Greenland Margin (Sinton and Duncan, 1998) indicating a possible causal relationship. A second relatively big shift can be observed right after C26n (~58.5 Ma) from ~14 to ~12.8 km/myr. In contrast to previous results, lowest values are reached in C25r with ~12 km/myr and persist at ~12.8 km/myr in the early Eocene. Spreading rates are lower in the latest Paleocene and early Eocene than predicted in GPTS2004 due to the underestimation of Chron C25r and C24r.

More surprisingly, we find a strong positive excursion in spreading rates exceeding 25 km/myr at Chron C28r. Even if we use the longest possible duration according to the record from Site 1262 of ~230 kyr for C28r, the spreading rates would be still at ~22 km/myr. This excursion can also be observed from duration estimates from the Zumaia (~19 to ~26 km/myr) and Bjala (~26 km/myr) land sections. If we assume a constant spreading rate between C29n and C28n for Site 1262 then the duration of C28r would have to be ~300 kyr. Cande and Kent (1992) identified relative uncertainties on the width of anomaly intervals ranging between 6.1 and 10% for anomaly 24 to 31. Variations in spreading rates calculated on the basis of the integrated Leg 208 magnetostratigraphy fall well within the relative uncertainties given by Cande and Kent (1992), except for Chron C28r. In order to arrive at an average spreading rate for C28r which is similar to spreading

rates above and below we have to reduce the C28r anomaly width from ~5.04 km (Cande and Kent, 1992) down to 3–3.5 km. This is outside the proposed error of Cande and Kent (1992) of ~10%. Here it is interesting to note that the widths of anomalies 28 and 29 have been selected from short sections of individual profiles from the North Pacific instead of taking the average of a stack (Cande and Kent, 1992). Based on our findings we suggest that the width of C28r is overestimated leading to the observed excursion in spreading rates. Hence, the apparent higher oscillations in spreading rates at C28r, C27n, and C26n are probably artifacts that result from the combined effects of relatively short, cycle-tuned polarity chrons and uncertainties in the corresponding magnetic anomaly widths in the South Atlantic synthesis profile as already observed for the Neogene part of the GPTS2004 (Ogg and Smith, 2004).

6. Conclusion

For the first time it is possible to establish a complete astronomically calibrated stratigraphic framework covering the entire Paleocene epoch (~66 to ~55 Ma) which is based on the identification of the stable long-eccentricity cycle (405-kyr). Our results show that the K/Pg boundary and the onset of the Paleocene–Eocene Thermal Maximum (PETM) are exactly 24 long eccentricity cycles or

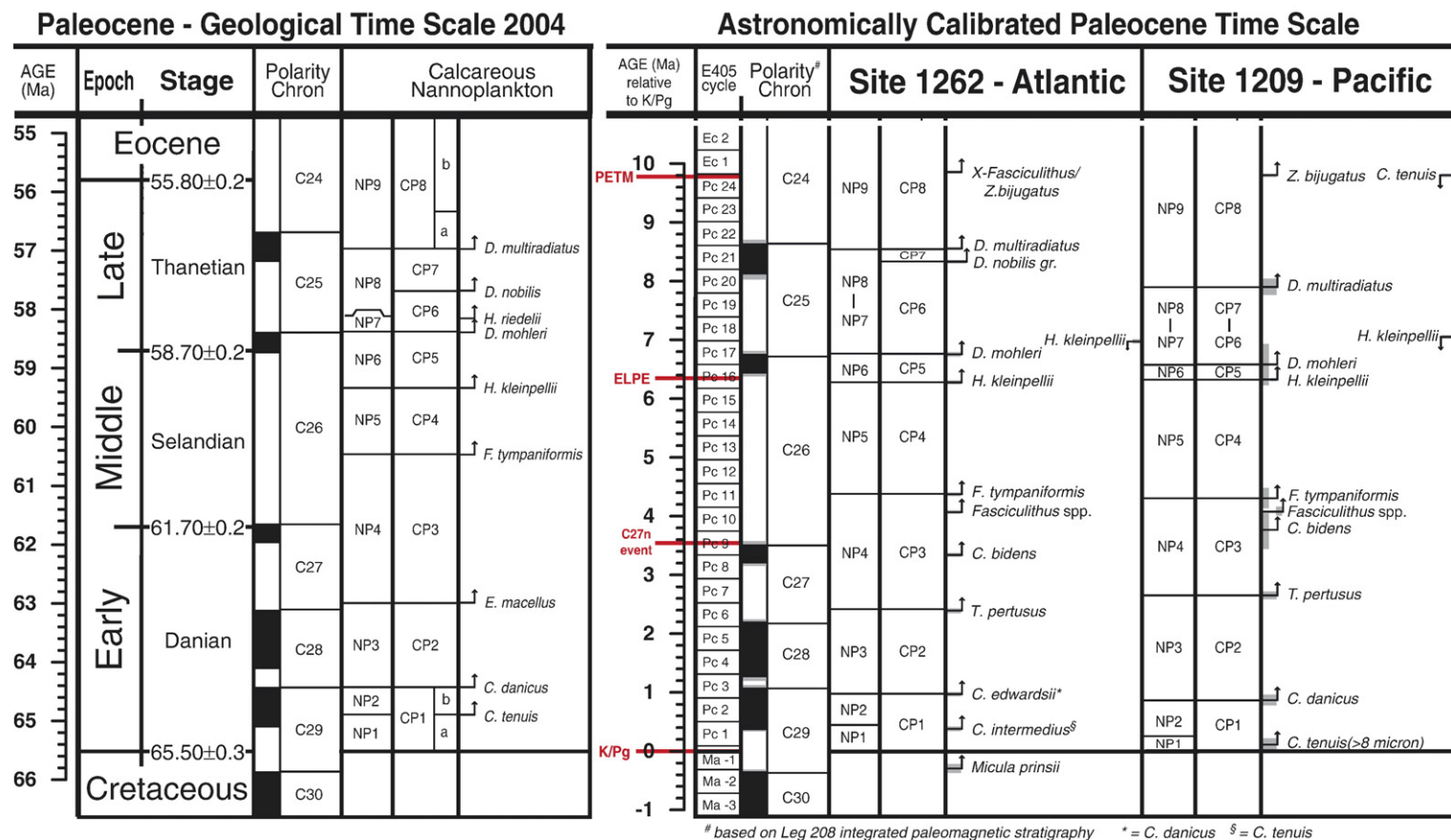


Table 4

Revised estimates for calcareous nannoplankton biostratigraphic datum levels at Sites 1262 and 1209 relative to the age of the K/Pg boundary

Event	Nannofossil marker	NP	CP	Top depth (mcd)	Bottom depth (mcd)	Mean depth (mcd)	Option_1		Option_2	
							Mean Age (ka)	Error (±) (kyr)	Mean Age (ka)	Error (±) (kyr)
ODP Leg 208 Site 1262										
CO	<i>Fasciculithus</i> / <i>Zygrhablithus</i>			139.78	139.81	139.80	55,466	2	55,871	3
LO	<i>D. multiradiatus</i>	NP9	CP8	154.50	154.71	154.61	56,759	7	57,159	7
LO	<i>D. nobilis</i>		CP7	157.24	157.45	157.35	56,968	11	57,379	12
HCO	<i>H. kleinpellii</i>			169.84	170.05	169.95	58,327	15	58,708	15
LO	<i>D. mohleri</i>	NP7	CP6	171.39	171.60	171.50	58,545	20	58,929	20
LO	<i>H. kleinpellii</i>	NP6	CP5	173.97	174.12	174.05	59,021	16	59,438	19
LO	<i>F. tympaniformis</i>	NP5	CP4	187.92	188.13	188.03	60,902	14	61,274	14
LO	<i>Fasciculithus</i> spp.			190.84	190.86	190.85	61,235	1	61,614	1
LO	<i>C. bidens</i>			196.74	196.95	196.85	61,948	13	62,322	13
LO	<i>T. pertusus</i>	NP4	CP3	203.56	203.76	203.66	62,895	21	63,273	22
LO	<i>C. edwardsii</i> (= <i>C. danicus</i>)	NP3	CP2	211.67	211.87	211.77	64,314	14	64,692	16
LO	<i>C. intermedius</i> (= <i>C. tenuis</i>)	NP2		214.81	215.02	214.92	64,905	25	65,274	27
Event	Nannofossil marker	NP	CP	Top depth (rmcd)	Bottom depth (rmcd)	Mean depth (rmcd)	Option_1		Option_2	
							Mean Age (ka)	Error (±) (kyr)	Mean Age (ka)	Error (±) (kyr)
ODP Leg 198 Site 1209										
LO	<i>Z. bijugatus</i>			217.95	218.00	217.97	55,517	10	55,986	7
HO	<i>C. tenuis</i>			217.95	218.00	217.97	55,517	10	55,986	7
LO	<i>D. multiradiatus</i>	NP9	CP8	227.30	228.80	228.05	57,403	117	57,799	114
HO	<i>H. kleinpellii</i>			231.80	233.23	232.51	58,258	128	58,639	127
LO	<i>D. mohleri</i>	NP7	CP6	233.23	235.71	234.47	58,719	335	59,110	338
LO	<i>H. kleinpellii</i>	NP6	CP5	235.71	237.26	236.48	59,217	163	59,653	195
LO	<i>F. tympaniformis</i>	NP5	CP4	243.26	244.76	244.01	60,982	156	61,354	160
LO	<i>Fasciculithus</i> spp.			244.76	245.27	245.02	61,205	57	61,591	58
LO	<i>C. bidens</i>			245.27	248.44	246.85	61,519	282	61,903	281
LO	<i>T. pertusus</i>	NP4	CP3	251.26	251.55	251.40	62,633	46	63,022	48
LO	<i>C. danicus</i>	NP3	CP2	256.40	257.04	256.72	64,403	70	64,791	72
LO	<i>C. tenuis</i> (> 8 µm)	NP2	CP1b	260.09	261.49	260.79	65,151	82	65,538	88

Note: HO = Highest Occurrence; LO = Lowest Occurrence, CO = Common Occurrence, HCO = Highest Common Occurrence; error takes in account only the sampling distance.

9720 kyr apart. We established a high-resolution calcareous nannofossil biostratigraphy for the South Atlantic and Pacific (Fig. 12, Table 4) that improves the available “standard” Paleocene biostratigraphic resolution allowing a much more detailed relative scaling of stages with biozones. Comparison with previous estimates for the absolute age of the K/Pg boundary and the PETM clearly show inconsistencies between astronomical calibrations and radiometric dating. The evolving dating dilemma is related to the uncertainty in the orbital solutions and to the uncertainty in the absolute age of the Fish Canyon Tuff dating monitor. The extraordinary accuracy of the new integrated Leg 208 chronostratigraphy both significantly refines the duration of magnetochrons and improves the GPTS.

Acknowledgements

Funding for this research was provided by the Deutsche Forschungsgemeinschaft (DFG) to U. Röhl and T. Westerhold; by the Joint Oceanographic Institutions/United States Science Support Program to J. Bowles and H. Evans; by Italian Murst-PRIN to I. Raffi, E. Fornaciari, S. Monechi and V. Reale. We thank T. Bralower, J. G. Ogg, and J. Laskar for discussions. We are indebted to H. Pfletschinger and V. Lukies (Bremen) for assisting in XRF scanning of Leg 208 cores, T. Frederichs (Bremen) for palaeomagnetic analyses, and the staff at GCR and BCR (IODP Core Repositories) for core handling. This research used samples and data provided by the Ocean Drilling Program (ODP). ODP is sponsored by the U.S. National

Science Foundation (NSF) and participating countries under the management of Joint Oceanographic Institution (JOI) Inc. The complete data set presented in this paper is available online in the WDC-MARE PANGAEA database under www.pangaea.de (<http://doi.pangaea.de/10.1594/PANGAEA.667122>). We thank two anonymous reviewers for their insightful reviews.

Appendix A. Supplementary data

Supplementary data associated with this article can be found, in the online version, at [doi:10.1016/j.palaeo.2007.09.016](https://doi.org/10.1016/j.palaeo.2007.09.016).

References

- Agnini, C., Fornaciari, E., Raffi, I., Rio, D., Rohl, U., Westerhold, T., 2007. High-resolution nannofossil biochronology of middle Paleocene to early Eocene at ODP Site 1262: implications for calcareous nannoplankton evolution. *Marine Micropaleontology*, 64 (3–4), 215–248. doi:10.1016/j.marmicro.2007.05.003.
- Alegret, L., Thomas, E., 2007. Deep-Sea environments across the Cretaceous/Paleogene boundary in the eastern South Atlantic Ocean (ODP Leg 208, Walvis Ridge). *Marine Micropaleontology*, 64 (1–2), 1–17.
- Agterberg, F.P., 2004. Geomathematics. In: Gradstein, F., Ogg, J., Smith, A. (Eds.), *A Geological Timescale 2004*, pp. 106–125.
- Bernaola, G., Monechi, S., 2007. Calcareous nannofossil extinction and survivorship across the Cretaceous/Paleogene boundary at Walvis Ridge (ODP Hole 1262C, South Atlantic Ocean). *Palaeogeography, Palaeoclimatology, Palaeoecology*. doi:10.1016/j.palaeo.2007.02.045.
- Bernaola, G., Baceta, J.I., Payros, A., Orue-Etxebarria, X., Appellaniz, E., 2006. The Paleocene and lower Eocene of the Zumaia section (Basque Basin). *Climate and Biota of the Early Paleogene 2006*. Post Conference Field Trip Guidebook, Bilbao. 82 pp.
- Bernaola, G., Baceta, J.I., Orue-Etxebarria, X., Alegret, L., Martin-Rubio, M., Arostegui, J., Dinarès-Turell, J., 2007. Evidence of an abrupt environmental disruption during the mid-Paleocene biotic event (Zumaia section, western Pyrenees). *GSA Bulletin*, 119 (7), 785–795.
- Bowles, J., 2006. Data report: Revised magnetostratigraphy and magnetic mineralogy of sediments from Walvis Ridge, Leg 208. In: Kroon, D., Zachos, J.C., Richter, C. (Eds.), *Proceedings of the Ocean Drilling Program. Scientific Results*, vol. 208 [Online]. Available from World Wide Web: <http://www-odp.tamu.edu/publications/208_SR/206/206.htm>.
- Bown, P., 2005. Selective calcareous nannoplankton survivorship at the Cretaceous–Tertiary boundary. *Geology*, 33 (8), 653–656.
- Bralower, T.J., 2005. Data report: Paleocene–early Oligocene calcareous nannofossil biostratigraphy, ODP Leg 198 Sites 1209, 1210, and 1211 (Shatsky Rise, Pacific Ocean). In: Bralower, T.J., Premoli Silva, I., Malone, M.J. (Eds.), *Proceedings of the Ocean Drilling Program. Scientific Results*, vol. 198 [Online]. Available from World Wide Web: <http://www-odp.tamu.edu/publications/198_SR/115/115.htm>.
- Bralower, T.J., Premoli Silva, I., Malone, M.J., et al., 2002a. *Proceedings of the Ocean Drilling Program. Initial Reports*, vol. 198. Texas A&M University, College Station TX 77845-9547, USA. [CD-ROM]. Available from: Ocean Drilling Program.
- Bralower, T.J., Premoli Silva, I., Malone, M.J., Scientific Participants of Leg 198, 2002b. New evidence for abrupt climate change in the Cretaceous and Paleogene: an ocean drilling program expedition to Shatsky Rise, northwest Pacific. *GSA Today*, 12 (11), 4–10.
- Bralower, T.J., Premoli Silva, I., Malone, M.J., 2006. Leg 198 synthesis: A remarkable 120-m.y. record of climate and oceanography from Shatsky Rise, northwest Pacific Ocean. In: Bralower, T.J., Premoli Silva, I., Malone, M.J. (Eds.), *Proceedings of the Ocean Drilling Program. Scientific Results*, vol. 198 [Online]. Available from World Wide Web: http://www-odp.tamu.edu/publications/198_SR/synth/synth.htm.
- Bukry, D., 1973. Low-latitude coccolith biostratigraphic zonation. In: Edgar, N.T., Saunders, J.B., et al. (Eds.), *Initial Rep. DSDP*, vol. 15. Washington, U.S. Government Printing Office, pp. 685–703.
- Bukry, D., 1978. Coccolith and silicoflagellate stratigraphy, northwestern Pacific Ocean, Deep Sea Drilling Project Leg 32. In: Larson, R.L., Moberly, R., et al. (Eds.), *Initial Rep. DSDP 32*. Washington, U.S. Government Printing Office, pp. 677–701.
- Cande, S.C., Kent, D.V., 1992. A new geomagnetic polarity time scale for the late Cretaceous and Cenozoic. *Journal of Geophysical Research*, 97 (B10), 13,917–13,951.
- Cande, S.C., Kent, D.V., 1995. Revised calibration of the geomagnetic polarity timescale for the Late Cretaceous and Cenozoic. *Journal of Geophysical Research*, 100 (B4), 6093–6095.
- Coxall, H.K., Wilson, P.A., Palike, H., Lear, C.H., Backman, J., 2005. Rapid stepwise onset of Antarctic glaciation and deeper calcite compensation in the Pacific Ocean. *Nature*, 433 (7021), 53–57.
- Cramer, B.S., 2001. Latest Paleocene–earliest Eocene cyclostratigraphy: using core photographs for reconnaissance geophysical logging. *Earth and Planetary Science Letters*, 186, 231–244.
- Cramer, B.S., Wright, J.D., Kent, D.V., Aubry, M.-P., 2003. Orbital climate forcing of $\delta^{13}\text{C}$ excursions in the late Paleocene–Eocene (chrons C24n–C25n). *Paleoceanography*, 18 (4), 1097. doi:10.1029/2003PA000909.
- D'Hondt, S., Herbert, T.D., King, J., Bibson, C., 1996a. Planktic foraminifera, asteroids, and marine production: Death and recovery at the Cretaceous–Tertiary boundary. In: Ryder, G., Fastovsky, D., Bartner, S. (Eds.), *The Cretaceous–Tertiary Event and Other Catastrophes in Earth History*. Boulder, Colorado, Geological Society of America Special Paper, pp. 303–317.
- D'Hondt, S., King, J., Bibson, C., 1996b. Oscillatory marine response to the Cretaceous–Tertiary impact. *Geology*, 24 (7), 611–614.
- Dinarès-Turell, J., Baceta, J.I., Pujalte, V., Orue-Etxebarria, X., Bernaola, G., 2002. Magnetostratigraphic and cyclostratigraphic calibration of a prospective Paleocene/Eocene stratotype at Zumaia (Basque Basin, northern Spain). *Terra Nova*, 14, 371–378.
- Dinarès-Turell, J., Baceta, J.I., Pujalte, V., Orue-Etxebarria, X., Bernaola, G., Lorito, S., 2003. Untangling the Paleocene climatic rhythm: an astronomically calibrated Early Paleocene magnetostratigraphy and biostratigraphy at Zumaia (Basque basin, northern Spain). *Earth and Planetary Science Letters*, 216, 483–500.
- Evans, H.F., Westerhold, T., Channell, J.E.T., 2004. ODP Site 1092: revised composite depth section has implications for Upper Miocene 'cryptochron'. *Geophysical Journal International*, 156 (2), 195–199.
- Gradstein, F., Ogg, J.G., Smith, A.G., 2004. Construction and summary of the geological time scale. In: Gradstein, F., Ogg, J.G., Smith, A.G. (Eds.), *A Geological Timescale 2004*. Cambridge, Cambridge University Press, pp. 455–464.
- Hallam, A., Hancock, J.M., LaBreque, J.L., Lowrie, W., Channell, J.E.T., 1985. Jurassic to Paleogene: Part I. Jurassic and Cretaceous geochronology and Jurassic to Paleogene magnetostratigraphy. In: Snelling, N.J. (Ed.), *The Chronology of the Geological Record*,

- Geological Society of London Memoir. Geological Society, London, pp. 118–140.
- Hancock, H.J.L., Dickens, G.R., 2005. Carbonate dissolution episodes in Paleocene and Eocene sediment, Shatsky Rise, west–central Pacific. In: Bralower, T.J., Premoli Silva, I., Malone, M.J. (Eds.), *Proceedings of the Ocean Drilling Program. Scientific Results*, vol. 198 [Online]. Available from World Wide Web: <http://www-odp.tamu.edu/publications/198_SR/116/116.htm>.
- Hay, W.W., DeConto, R., Wold, C.N., Wilson, K.M., Voigt, S., Schulz, M., Wold-Rosby, A., Dullo, W.-C., Ronov, A.B., Balukhovskiy, A.N., Soeding, E., 1999. Alternative global Cretaceous paleogeography. In: Barrera, E., Johnson, C. (Eds.), *The Evolution of Cretaceous Ocean/Climate Systems*. Geological Society of America Special Paper, pp. 1–47.
- Herbert, T.D., 1999. Towards a composite orbital chronology for the Late Cretaceous and Early Paleogene GPTS. In: Shackleton, N.J., McCave, I.N., Weedon, G.P. (Eds.), *Philosophical Transactions of the Royal Society of London. A* 1891–1905.
- Herbert, T.D., D'Hondt, S.L., 1990. Precessional climate cyclicity in Late Cretaceous–Early Tertiary marine sediments: a high resolution chronometer of Cretaceous–Tertiary boundary events. *Earth and Planetary Science Letters*, 99, 263–275.
- Herbert, T.D., Premoli-Silva, I., Erba, E., Fischer, A.G., 1995. Orbital Chronology of Cretaceous–Paleocene Marine Sediments. In: Berggren, W.A., Kent, D.V., Aubry, M.P., Hardenbol, J. (Eds.), *Geochronology, Time Scales and Global Stratigraphic Correlation*. Spec. Publ., SEPM, pp. 81–93.
- Hicks, J.F., Johnson, K.R., Obradovich, J.D., Tauxe, L., Clark, D., 2002. Magnetostratigraphy and geochronology of the Hell Creek and basal Fort Union Formations of southwestern North Dakota and a recalibration of the age of the Cretaceous–Tertiary boundary. In: Hartman, J.H., Johnson, K.R., Nichols, D.J. (Eds.), *The Hell Creek Formation and the Cretaceous–Tertiary boundary in the northern Great Plains: An integrated continental record of the end of the Cretaceous*. Boulder, Colorado, Geological Society of America Special Paper, pp. 35–55.
- Hilgen, F., Brinkhuis, H., Zachariasse, W.-J., 2006a. Unit stratotypes for global stages: The Neogene perspective. *Earth-Science Reviews*, 74 (1–2), 113–125.
- Hilgen, F.J., Krijgsman, W., Kuiper, K.F., Lourens, L.J., Wijbrans, J.R., 2006b. Astronomical calibration of geological time, EGU 2006. *Geophysical Research Abstracts*, Vienna.
- Hsü, K.J., He, Q.X., McKenzie, A., 1982. Terminal Cretaceous environmental and evolutionary changes. In: Silver, L.T., Schultz, P.H. (Eds.), *Geological implications of impacts of large asteroids and comets on the Earth*. Geological Society of America Special Paper, pp. 317–328.
- Jansen, J.H.F., Van der Gaast, S.J., Koster, B., Vaars, A.J., 1998. CORTEX, a shipboard XRF-scanner for element analyses in split sediment cores. *Marine Geology*, 151 (1–4), 143–153.
- Kirschvink, J.L., 1980. The least-squares line and plane and the analysis of paleomagnetic data. *Geophysical Journal of the Royal Astronomical Society*, 62, 699–718.
- Kuiper, K.F., Hilgen, F.J., Steenbrink, J., Wijbrans, J.R., 2004. $^{40}\text{Ar}/^{39}\text{Ar}$ ages of tephras intercalated in astronomically tuned Neogene sedimentary sequences in the Mediterranean. *Earth and Planetary Science Letters*, 222, 583–597.
- Kuiper, K.F., Wijbrans, J.R., Hilgen, F.J., 2005. Radioisotopic dating of the Tortonian Global Stratotype Section and Point: implications for intercalibration of $^{40}\text{Ar}/^{39}\text{Ar}$ and astronomical dating methods. *Terra Nova*, 17 (4), 385–398.
- Kroon, D., Zachos, J.C., et al., 2007. Leg 208 synthesis: Cenozoic climate cycles and excursions. *Proceedings of the Ocean Drilling Program. Scientific Results*, vol. 208. Ocean Drilling Program, College Station, TX. doi:10.2973/odp.proc.sr.208.201.2007. 55 pp.
- Laskar, J., 1999. The limits of Earth orbital calculations for geological time-scale use. In: Shackleton, N.J., McCave, I.N., Weedon, G.P. (Eds.), *Philosophical Transactions of the Royal Society of London. A*, 1735–1759.
- Laskar, J., Robutel, P., Joutel, F., Gastineau, M., Correia, A., Levrard, B., 2004. A long-term numerical solution for the insolation quantities of the Earth. *Astronomy and Astrophysics*, 428, 261–285.
- Lees, J.A., Bown, P.R., 2005. Upper Cretaceous calcareous nannofossil biostratigraphy, ODP Leg 198 (Shatsky Rise, northwest Pacific Ocean). In: Bralower, T.J., Premoli Silva, I., Malone, M.J. (Eds.), *Proceedings of the Ocean Drilling Program. Scientific Results*, vol. 198 [Online]. Available from World Wide Web: <http://www-odp.tamu.edu/publications/198_SR/114/114.htm>.
- Lourens, L.J., Hilgen, F.J., Laskar, J., Shackleton, N.J., Wilson, D., 2004. The Neogene Period. In: Gradstein, F., Ogg, J., Smith, A. (Eds.), *A Geological Timescale 2004*, pp. 409–440.
- Lourens, L.J., Sluijs, A., Kroon, D., Zachos, J.C., Thomas, E., Rohl, U., Bowles, J., Raffi, I., 2005. Astronomical pacing of late Palaeocene to early Eocene global warming events. *Nature*, 435 (7045), 1083–1087.
- Luterbacher, H.P., Ali, J.R., Brinkhuis, H., Gradstein, F.M., Hooker, J.J., Monechi, S., Ogg, J.G., Powell, J., Röhl, U., Sanfilippo, A., Schmitz, B., 2004. The Paleogene Period. In: Gradstein, F., Ogg, J., Smith, A. (Eds.), *A Geological Timescale 2004*, pp. 384–408.
- Machlus, M., Hemming, S.R., Olsen, P.E., Christie-Blick, N., 2004. Eocene calibration of geomagnetic polarity time scale reevaluated: evidence from the Green River Formation of Wyoming. *Geology*, 32 (2), 137–140.
- Martini, E., 1971. Standard Tertiary and Quaternary calcareous nannoplankton zonation. In: Farinacci, A. (Ed.), *2nd Int. Conf. Planktonic Microfossils Roma, Rome* (Ed. Tecnosci.), pp. 739–785.
- Min, K., Mundil, R., Renne, P.R., Ludwig, K.R., 2000. A test for systematic errors in $^{40}\text{Ar}/^{39}\text{Ar}$ geochronology through comparison with U/Pb analysis of a 1.1-Ga rhyolite. *Geochimica et Cosmochimica Acta*, 64 (1), 73–98.
- Mukhopadhyay, S., Farley, K.A., Montanari, A., 2001. A short duration of the Cretaceous–Tertiary boundary event: evidence from extraterrestrial helium-3. *Science*, 291 (5510), 1952–1955. doi:10.1126/science.291.5510.1952.
- Okada, H., Bukry, D., 1980. Supplementary modification and introduction of code numbers to the low-latitude coccolith biostratigraphic zonation (Bukry, 1973; 1975). *Marine Micropaleontology*, 5, 321–325.
- Ogg, J.G., Bardot, L., 2001. Aptian through Eocene magnetostratigraphic correlation of the Blake Nose Transect (Leg 171B), Florida Continental Margin. In: Kroon, D., Norris, R.D., Klaus, A. (Eds.), *Proceedings of the Ocean Drilling Program. Scientific Results*, vol. 171B, 1–58 [Online], http://www-odp.tamu.edu/publications/171B_SR/Volume/Chapters/SR171B09.pdf.
- Ogg, J.G., Smith, A.G., 2004. The geomagnetic polarity time scale. In: Gradstein, F., Ogg, J., Smith, A. (Eds.), *A Geological Timescale 2004*. Cambridge University Press, pp. 63–86.
- Paillard, D., Labeyrie, L., Yiou, P., 1996. Macintosh program performs time-series analysis. *Eos Trans. AGU*, v. 77, no. 379. p. (http://www.agu.org/eos_elec/96097e.html).
- Pälike, H., Shackleton, N.J., Röhl, U., 2001. Astronomical forcing in Late Eocene marine sediments. *Earth and Planetary Science Letters*, 193, 589–602.

- Pälike, H., Laskar, J., Shackleton, N.J., 2004. Geologic constraints on the chaotic diffusion of the solar system. *Geology*, 32 (11), 929–932.
- Pälike, H., Norris, R.D., Herrle, J.O., Wilson, P.A., Coxall, H.K., Lear, C.H., Shackleton, N.J., Tripathi, A.K., Wade, B.S., 2006. The Heartbeat of the Oligocene Climate System. *Science*, 314 (5807), 1894–1898.
- Renne, P.R., Swisher, C.C., Deino, A.L., Karner, D.B., Owens, T.L., DePaolo, D.J., 1998. Intercalibration of standards, absolute ages and uncertainties in $^{40}\text{Ar}/^{39}\text{Ar}$ dating. *Chemical Geology*, 145, 117–152.
- Perch-Nielsen, K., 1985. Cenozoic calcareous nannofossils. In: Bolli, H.M., Saunders, J.B., Perch-Nielsen, K. (Eds.), *Plankton Stratigraphy*. Cambridge University Press, pp. 427–554.
- Petritzto, M.R., 2005. An early late Paleocene event on Shatsky Rise, northwest Pacific Ocean (ODP Leg 198): evidence from planktonic foraminiferal assemblages. In: Bralower, T.J., Premoli Silva, I., Malone, M.J. (Eds.), *Proceedings of the Ocean Drilling Program. Scientific Results*, vol. 198 [Online]. Available from World Wide Web: <http://www-odp.tamu.edu/publications/198_SR/102/102.htm>.
- Preissinger, A., Aslanian, S., Brandstatter, F., Grass, F., Stradner, H., Summesberger, H., 2002. Cretaceous–Tertiary profile, rhythmic deposition, and geomagnetic polarity reversals of marine sediments near Bjala, Bulgaria. In: Koeberl, C., MacLeod, K.G. (Eds.), *Catastrophic Events and Mass Extinctions: Impacts and Beyond*. *Geol. Soc. Am. Spec. Pap.*, pp. 213–229.
- Richter, T.O., Van der Gast, S., Koster, R., Vaars, A., Gieles, R., De Stigter, H.C., De Haas, H., Van Weering, T.C.E., 2006. The Avaatech XRF Core Scanner: technical description and applications to NE Atlantic sediments. In: Rothwell, R.G. (Ed.), *New Techniques in Sediments Core Analysis*. Geological Society London, Special Publication, London, pp. 39–51.
- Röhl, U., Abrams, L.J., 2000. High-Resolution, Downhole and Non-Destructive Core Measurements from Sites 999 and 1001 in the Caribbean Sea: Application to the Late Paleocene Thermal Maximum. In: Leckie, R.M., Sigurdsson, H., Acton, G.D., Draper, G. (Eds.), *Proceedings of the Ocean Drilling Program. Scientific Results*, vol. 165, 191–203.
- Röhl, U., Bralower, T.J., Norris, R.D., Wefer, G., 2000. New chronology for the late Paleocene thermal maximum and its environmental implications. *Geology*, 28 (10), 927–930.
- Röhl, U., Ogg, J.G., Geib, T.L., Wefer, G., 2001. Astronomical calibration of the Danian time scale. In: Kroon, D., Norris, R.D., Klaus, A. (Eds.), *Western North Atlantic Palaeogene and Cretaceous Palaeoceanography*. Geological Society Special Publications, London, pp. 163–183.
- Röhl, U., Norris, R.D., Ogg, J.G., 2003. Cyclostratigraphy of upper Paleocene and lower Eocene sediments at Blake Nose Site 1051 (western North Atlantic). In: Wing, S.L., Gingerich, P.D., Schmitz, B., Thomas, E. (Eds.), *Causes and Consequences of Globally Warm Climates in the Early Paleogene*. Geological Society of America Special Paper, Boulder: Colorado, pp. 576–589.
- Röhl, U., Westerhold, T., Bralower, T.J., Petritzto, M.-R., Zachos, J.C., 2004. An Early Late Paleocene Global Dissolution Event and New Constraints for an Astronomically-Tuned Early Paleogene Time Scale. Abstract. 8th International Conference on Paleoceanography, Biarritz, France.
- Röhl, U., Westerhold, T., Monechi, S., Thomas, E., Zachos, J.C., Donner, B., 2005. The Third and Final Early Eocene Thermal Maximum: Characteristics, Timing and Mechanisms of the "X" Event. *Geological Society of America*, p. 264. Abstracts with Programs.
- Schoene, B., Bowring, S.A., 2006. U–Pb systematics of the McClure Mountain syenite: thermochronological constraints on the age of the Ar-40/Ar-39 standard MMhb. *Contributions to Mineralogy and Petrology*, 151 (5), 615–630.
- Schoene, B., Crowley, J.L., Condon, D.J., Schmitz, M.D., Bowring, S.A., 2006. Reassessing the uranium decay constants for geochronology using ID-TIMS U–Pb data. *Geochimica et Cosmochimica Acta*, 70 (2), 426–445.
- Shackleton, N.J., Crowhurst, S.J., Weedon, G.P., Laskar, J., 1999. Astronomical calibration of Oligocene–Miocene time. In: Shackleton, N.J., McCave, I.N., Weedon, G.P. (Eds.), *Philosophical Transactions of the Royal Society of London. A*, pp. 1907–1929.
- Shackleton, N.J., Hall, M.A., Raffi, I., Tauxe, L., Zachos, J., 2000. Astronomical calibration age for the Oligocene–Miocene boundary. *Geology*, 28 (5), 447–450.
- Shipboard Scientific Party, 2002a. Explanatory notes. In: Bralower, T.J., Premoli Silva, I., Malone, M.J., et al. (Eds.), *Proceedings of the Ocean Drilling Program. Initial Reports*, vol. 198 [Online]. Available from World Wide Web: http://www-odp.tamu.edu/publications/198_IR/chap_02/chap_02.htm.
- Shipboard Scientific Party, 2002b. Leg 198 summary. In: Bralower, T.J., Premoli Silva, I., Malone, M.J., et al. (Eds.), *Proceedings of the Ocean Drilling Program. Initial Reports*, vol. 198. Texas A&M University, College Station TX 77845-9547, USA, pp. 1–148. [CD-ROM]. Available from: Ocean Drilling Program.
- Shipboard Scientific Party, 2004a. Explanatory notes. In: Zachos, J.C., Kroon, D., Blum, P., et al. (Eds.), *Proceedings of the Ocean Drilling Program. Initial Reports*, vol. 208. Texas A&M University, College Station TX 77845-9547, USA, pp. 1–63. [CD-ROM]. Available from: Ocean Drilling Program.
- Shipboard Scientific Party, 2004b. Leg 208 summary. In: Zachos, J.C., Kroon, D., Blum, P., et al. (Eds.), *Proceedings of the Ocean Drilling Program. Initial Reports*, vol. 208. Texas A&M University, College Station TX 77845-9547, USA, pp. 1–112. [CD-ROM]. Available from: Ocean Drilling Program.
- Sinton, C.W., Duncan, R.A., 1998. $^{40}\text{Ar}/^{39}\text{Ar}$ ages of lavas from the southeast Greenland margin, ODP Leg 152, and the Rockall Plateau, DSDP Leg 81. In: Larsen, H.C., Saunders, A.D., Clift, P.D. (Eds.), *Proceedings of the Ocean Drilling Program. Scientific Results*, vol. 152. Ocean Drilling Program, College Station, TX, pp. 387–401.
- Swisher, C., Turrin, B., Kuiper, K.F., 2006. Bringing the Paleogene in sync with the ATS, EGU 2006. *Geophysical Research Abstracts*, Vienna.
- ten Kate, W.G.H.Z., Sprenger, A., 1993. Orbital cyclicities above and below the Cretaceous/Paleogene boundary at Zumaya (N Spain), Agost and Rellu (SE Spain). *Sedimentary Geology*, 87, 69–101.
- Thomas, D.J., 2004. Evidence for deep-water production in the North Pacific Ocean during the early Cenozoic warm interval. *Nature*, 430 (6995), 65–68.
- Varadi, F., Runnegar, B., Ghil, M., 2003. Successive Refinements in Long-Term Integrations of Planetary Orbits. *Astrophysical Journal*, 592, 620–630.
- Villeneuve, M., 2004. Radiogenic isotope geochronology. In: Gradstein, F., Ogg, J., Smith, A. (Eds.), *A Geological Timescale 2004*. Cambridge University Press, pp. 87–95.
- Wade, B.S., Pälike, H., 2004. Oligocene climate dynamics. *Paleoceanography*, 19, PA4019. doi:10.1029/2004PA001042.
- Weedon, G.P., 1993. The recognition and stratigraphic implications of orbital-forcing of climate and sedimentary cycles. In: Wright, V.P., et al. (Eds.), *Sedimentology review*. Blackwell Scientific, pp. 31–50.
- Weedon, G.P., 2003. *Time-series Analysis and Cyclostratigraphy*. Cambridge University Press.

- Westerhold, T., Röhl, U., 2006. Data report: Revised composite depth records for Shatsky Rise Sites 1209, 1210, and 1211. In: Bralower, T.J., Premoli Silva, I., Malone, M.J. (Eds.), *Proceedings of the Ocean Drilling Program. Scientific Results*, vol. 198 [Online]. Available from World Wide Web: <http://www-odp.tamu.edu/publications/198_SR/122/122.htm>.
- Westerhold, T., Röhl, U., Laskar, J., Bowles, J., Raffi, I., Lourens, L.J., Zachos, J.C., 2007. On the duration of magnetochrons C24r and C25n and the timing of early Eocene global warming events: implications from the Ocean Drilling Program Leg 208 Walvis Ridge depth transect. *Paleoceanography*, 22, PA2201. doi:10.1029/2006PA001322.
- Zachos, J.C., Arthur, M.A., Dean, W.E., 1989. Geochemical evidence for suppression of pelagic marine productivity at the Cretaceous/Tertiary Boundary. *Nature*, 337 (61–64).
- Zachos, J.C., Wara, M.W., Bohaty, S., Delaney, M.L., Petrizzo, M.R., Brill, A., Bralower, T.J., Premoli-Silva, I., 2003. A transient rise in tropical sea surface temperature during the Paleocene–Eocene thermal maximum. *Science*, 302 (5650), 1551–1554.
- Zachos, J.C., Kroon, D., Blum, P., et al., 2004. *Proceedings of the Ocean Drilling Program. Initial Reports*, vol. 208. Texas A&M University, College Station TX 77845–9547, USA. [CD-ROM]. Available from: Ocean Drilling Program.
- Zachos, J.C., Röhl, U., Schellenberg, S.A., Sluijs, A., Hodell, D.A., Kelly, D.C., Thomas, E., Nicolo, M., Raffi, I., Lourens, L.J., McCarren, H., Kroon, D., 2005. Rapid acidification of the ocean during the Paleocene–Eocene thermal maximum. *Science*, 308 (5728), 1611–1615.